DeepWind Deliverable

Grant Agreement number: 256769

Project title: Future Deep Sea Wind Turbine Technologies

Deliverable No.: D 6.1

Deliverable title: Technical Report on the Physical Model Experiments

Deliverable status: Report

Name of lead beneficiary: DHI

Nature of deliverable: R

Dissemination level: PU

Due date from Annex 1: M9

Actual submission date: 31 October 2012

Quality check approval by: 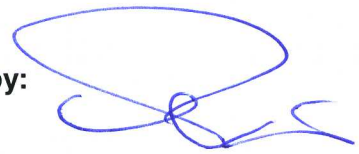 **date:** 29/10 - 2012

256769 - DEEPWIND

Technical Report on the Physical Model Experiments

Deliverable 6.1

256769 - DEEPWIND

Technical Report on the Physical Model Experiments

Deliverable 6.1

EC-FP7-FET
Report
October 2012

This project was delivered under the DHI Business Management System certified by DNV to be in compliance with ISO 9001: Quality Management System

256769 - DEEPWIND

Technical Report on the Physical Model Experiments

Deliverable 6.1

October 2012

Agern Allé 5
DK-2970 Hørsholm
Denmark

Tel: +45 4516 9200
Fax: +45 4516 9292
dhi@dhigroup.com
www.dhigroup.com

Client	Client's representative
EC-FP7-FET [ENERGY.2010.10.2-1]	Mr Thierry D'Estangtoi

Project	Project No
DEEPWIND	11807547
Authors Stefan Carstensen	Date 31 October 2012
	Approved by Jesper Fuchs Head of Projects, POT

Revision	Description	By	Checked	Approved	Date
C	Report	SCA	JUF	JUF	31.10.12
B	Draft Report	SCA	EDC/MHE	JUF	07.03.12
A	Working Draft Report	SCA			15.12.11

Key words	Classification
Cylinder Forces VAWT	☐ Open ☐ Internal ☒ Proprietary

Distribution		No of copies
EU:	Mr Thierry D'Estangtoi	PDF
	Partners	PDF
DHI:	SCA – XEM – JTS	PDF

CONTENTS

DRAWINGS

APPENDICES

1 INTRODUCTION

This report is Deliverable 6.1 “Technical report on the physical model experiments” under Work Package 6 of the DEEPWIND project.

The DEEPWIND project is a collaborative research project on future deep sea wind turbine technologies and is partially funded by the European Commission (EC) through the 7th Framework Programme (FP7), EC-FP7-FET [ENERGY.2010.10.2-1]. Project work was started on 1 October 2010 after accession by DHI of Grant Agreement no: 256769 between the EC and the DEEPWIND consortium, which is coordinated by DTU Wind Energy (formerly RISØ DTU) and consists of DHI and 10 additional partners.

Work Package 6 of the DEEPWIND project concerns forces on a rotating circular cylinder in water. The circular cylinder represents the submerged part of the novel floating wind turbine concept proposed in /1/ and studied in the DEEPWIND project. The floating wind turbine concept, in the following denoted the DEEPWIND concept, is shown in Figure 1.1.

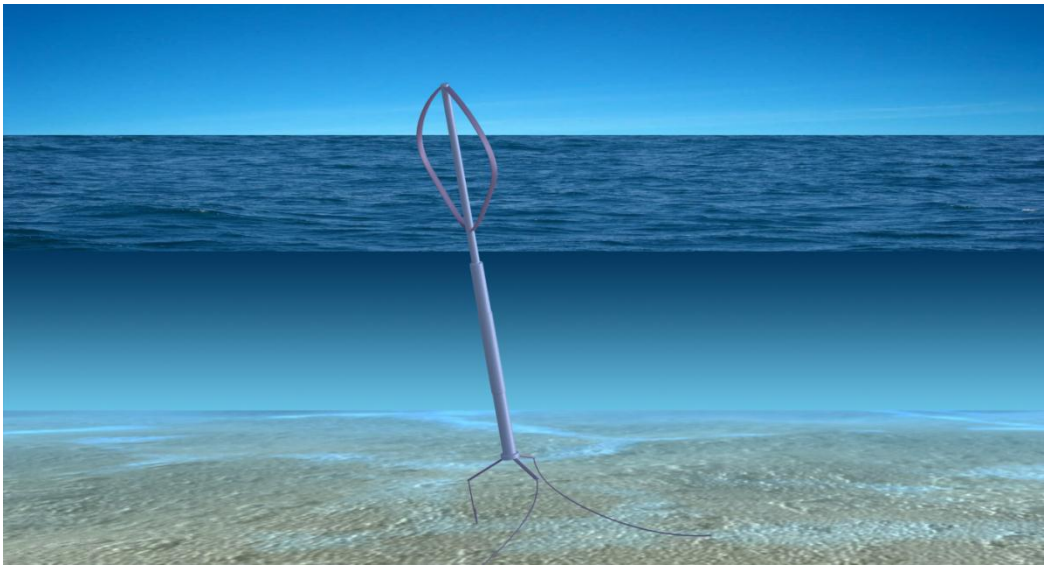

Figure 1.1 Artists illustration of the DEEPWIND concept.

Work Package 6 utilises physical laboratory tests (Deliverable 6.1) to establish the physics and address possible scaling effects with refined numerical modelling (Deliverable 6.2). The results are then analysed and parameterised as a basis for the engineering model (Deliverable 6.3). The present report describes the laboratory tests and results. The conclusion (Section 2) is kept short and expanded upon in Deliverable 6.3 (“Description of Engineering Model”).

2 EXECUTIVE SUMMARY

Forces on a rotating circular cylinder in unsteady flows have been measured experimentally.

The results show that the cross-flow (lift) force to a first approximation may be represented by a formulation similar to the well-known Morison formulation. The lift force is found to be almost in phase with the free-stream velocity and depends on the ratio between the surface speed of the cylinder and the outer flow velocity. The variation of the lift force with the phase of the wave motion was shown to be predicted by potential flow theory for KC < 8. However, the magnitude of the lift force was substantially smaller than that predicted by potential flow theory. The magnitude of the lift force was found to be in the order of (0.5 to 2 times) the in-line hydrodynamic mass force. The hydrodynamic mass force is proportional to the acceleration which means that there is a phase difference of almost 90 degrees between the in-line force and the cross-flow force for KC < 8.

The in-line force was also investigated. The cylinder rotation did not change the in-line force significantly for small KC numbers and wave-dominated combined wave and current. The in-line force, however, was shown to change with increasing current component.

The friction torque opposing the cylinder rotation was measured in stagnant water and for various combined wave and current conditions. The friction torque in stagnant water was shown to compare with previous studies; and the friction torque opposing the cylinder rotation, under wave action, was found to be of the same order of magnitude as that for rotation alone.

3 EXPERIMENTAL FACILITY

3.1 General

The experimental setup included a section of a circular cylinder, the model spar buoy, mounted to a carriage on rails atop of a current flume. Current was directed through the flume, while the effect of waves was included by an oscillatory movement of the carriage. At the same time the model was rotating in the water. Due to experimental constraints only co-linear current and waves can be tested in the physical model experiments

3.2 Current Flume

A sketch of the current flume is given in Figure 3.1 and a picture is given in Figure 3.2. It is a 35 m long, 3 m wide, and 1 m deep flume. A carriage running on rails on top of the flume can operate at up to 2 m/s.

The global coordinate system (X; Y; Z) was arranged so that X was in the stream-wise direction. Z was vertical, positive direction upwards, and Y was in the transverse direction according to the right-hand-rule.

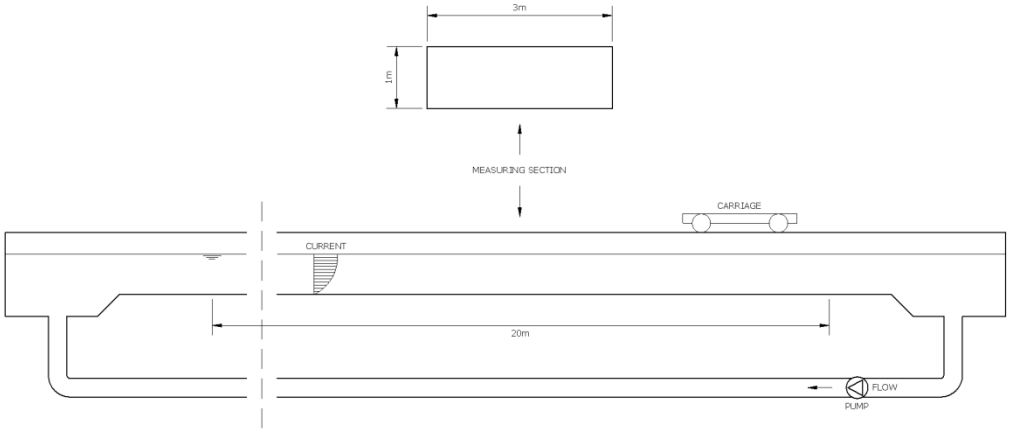

Figure 3.1 Schematic description of the current flume.

Figure 3.2 Current flume with carriage on top. The side walls are made of glass over a part of the measuring section allowing side view inspection.

3.2.1 Blockage

The relatively large size of the experimental facility was important as the side wall of the experimental facility induces a confining effect on the model (see Section 4), which normally is termed *blockage*. Generally, one may assume that the blockage effect is small and may be ignored when the ratio of the cylinder diameter to the width of the experimental facility, D/B, is less than 0.1. In the present situation blockage effects were undesirable and the ratio D/B was therefore kept below 0.1.

3.3 Test Set-up

The typical dimension for the submerged rotating shaft has been addressed in Milestone 11 (/2/) and in follow-up e-mail dated 31-05-2011. Table 3.1 summarises the typical shaft diameter and rotational speed.

Table 3.1 Summary of typical shaft diameter and rotational speed, reproduced from /2/ and follow-up e-mail on the shaft diameter dated 31-05-2011.

Property	**Variable name / Unit**	**Range**		
		Lower limit	2 MW	Upper limit
Diameter	D (m)	6	8 (9)	13
Rotational speed	f (rpm)	0	15	20
Rotational speed	f (Hz)	0	0.25	0.33
Angular frequency	$\omega = 2\pi f$ (rad/s)	0	1.6	2.1

A scale model of the submerged rotating shaft was modelled by a circular cylinder considering the restraints imposed by the experimental facility (see Sections 3.2.1 and 4); the circular cylinder was suspended via ball bearings and a support frame from the carriage, see Figure 3.3.

The rotating circular cylinder was subject to different current conditions, wave conditions and combined wave and current conditions.

Current was generated by pumping water through the flume while waves were simulated by moving the carriage. Simulating wave motion with a carriage means that the elliptical orbital motion of water particles under real waves was neglected as the motion of water particles is simulated as straight-line oscillatory motion.

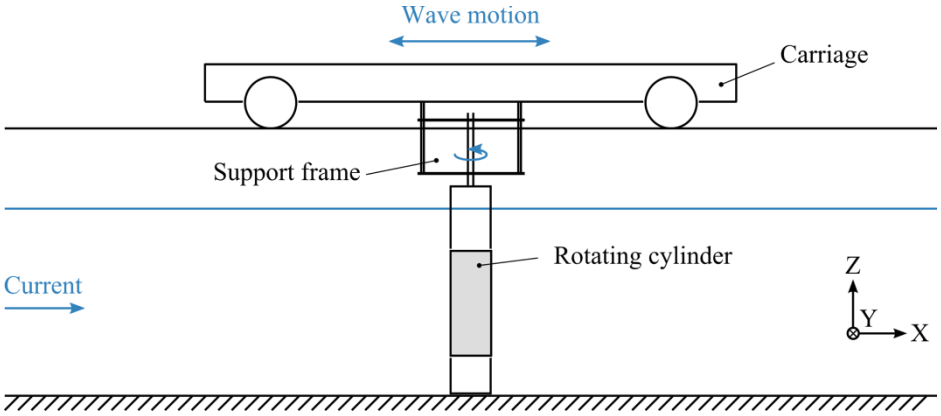

Figure 3.3 Schematic drawing of model submerged rotating cylinder mounted via ball bearing and support frame to the carriage.

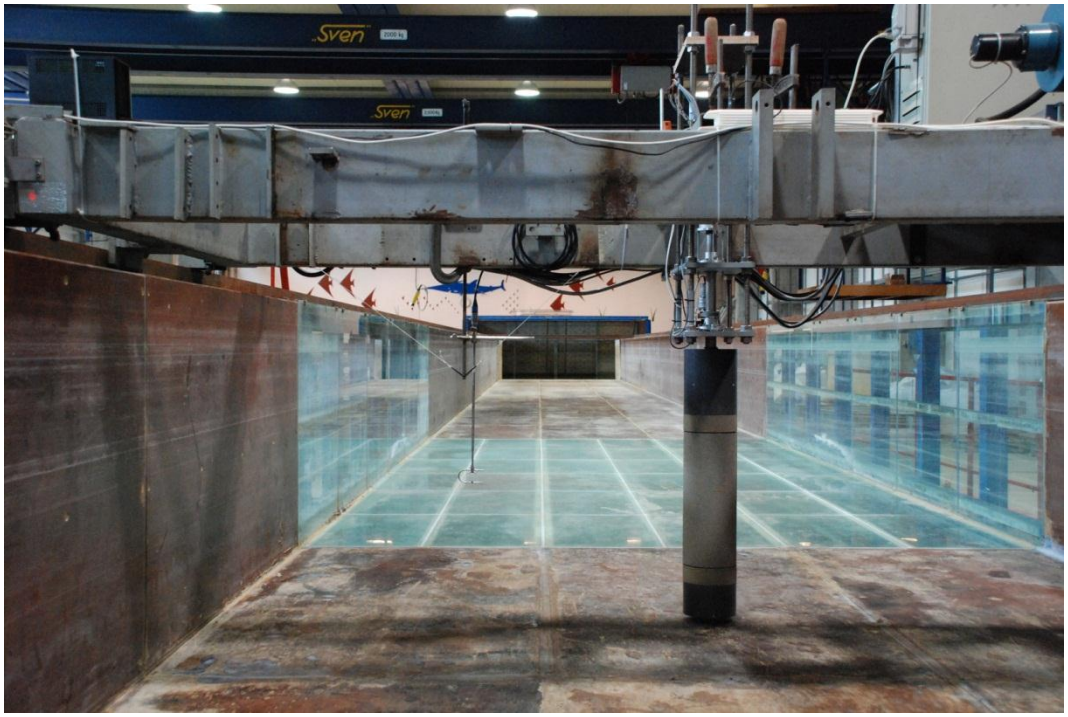

Figure 3.4 Rotating cylinder mounted via ball bearings and support frame to carriage

4 MODEL AND MODEL SCALE

4.1 Model Laws

The flow around the rotating shaft may be broken down into two classical topics within hydrodynamics:

a) Flow around a circular cylinder in current and waves
b) Steady flow around a rotating circular cylinder

The flow around a non-rotating circular cylinder in current and waves exerts a resultant in-line force (drag) and cross-flow force (lift) on the cylinder. Cylinder diameter, surface roughness and inclination all influence the resultant force just as current speed and amplitude of the wave motion do. Generally, the effect of cylinder diameter, D, current speed, U, and the amplitude of the wave motion, a, is expressed in terms of two non-dimensional numbers: the Reynolds number, $Re = DU/\nu$, and the Keulegan-Carpenter number, $KC = 2\pi a/D$. Surface roughness is expressed in terms of the relative roughness, k_s/D, where k_s is the equivalent sand roughness.

A rotating cylinder in steady current experiences an additional force perpendicular to the motion (lift) known as the Magnus effect. Furthermore, the wall shear stress on the cylinder surface exerts a resultant friction opposite the cylinder rotation. The rotation may be expressed as the ratio of peripheral speed and the free stream velocity, $\alpha = \omega R/U$.

Due to mutually exclusive scaling laws dynamic similarity between physical model experiments and full-scale is only attainable at full-scale. The physical model experiments were scaled using Froude scaling. Froude scaling together with geometrical similarity allowed reproduction of the KC, α and k_s/D in the model. This, however, means that the Reynolds number was not scaled correctly in the physical model experiments. The consequences of this may, however, be limited (see e.g. Section 7.2) because of the surface roughness.

4.2 Model Scale

The physical model experiments were scaled according to Froude number scaling as detailed in Section 4.1.

$$Fr_{full-scale} = Fr_{model}$$

$$\left(\frac{u}{\sqrt{gh}}\right)_{full-scale} = \left(\frac{u}{\sqrt{gh}}\right)_{model}$$

However, all data and results are presented in model scale in this report. Table 4.1 gives factors for scaling of full-scale to model scale.

Table 4.1 Factors for scaling of full-scale to model scale assuming difference in water density of S = $\rho_{full\text{-}scale}/\rho_{model}$ = 1035/1000 =1.035.

Parameter	Scale Law	Scale Factor (λ = 50)	
Length	Λλ	50	
Area	λ^2	2,500	
Volume	λ^3	125,000	
Time	$\lambda^{1/2}$	7.1	
Velocity	$\lambda^{1/2}$	7.1	
Mass	$S\lambda^3$	129,375	
Force	$S\lambda^3$	129,375	
Moment	$S\lambda^4$	6,468,750	
Pressure	λ	50	

4.3 Submerged Rotating Circular Cylinder

Figure 4.1 shows the submerged rotating circular cylinder. The cylinder is suspended from an adjustable support frame, which allowed the vertical position of the cylinder in the water column to be adjusted. A close-up of the support frame is shown in Figure 4.2. The support frame consisted of two box profiles (placed on top of the carriage), four M20 threaded steel rods and two 200 mm x 400 mm x 15 mm steel plates assembled with nuts and washers.

Figure 4.1 Submerged rotating circular cylinder

Figure 4.2 Close-up of the support frame: (left) side view and (right) camera pointing in the positive X-direction, the stream-wise direction.

The submerged rotating circular cylinder was split into three parts. The middle part is the measuring section while the bottom and top parts are dummy sections. The dummy sections were rigidly fixed to the drive shaft (Figure 4.1 and Figure 4.3) while the measuring section was suspended in two 2-component force gauges. One force gauge was inside the bottom dummy section and the other was inside the top dummy section. Figure 4.3 shows a sketch of the cylinder with the two dummy sections removed. One end of each of the two force gauges was rigidly fixed to the drive shaft, while the other end of the force gauges held the measuring section. A small gap between the top and bottom cap of the measuring section allowed for slight movement of the measuring section relative to the drive shaft so that the displacement could be measured by the strain gauges on the force gauges. The two force gauges are placed off-centre, as shown in Figure 4.3, to also measure the friction from torque of the cylinder as well as the two normal forces.

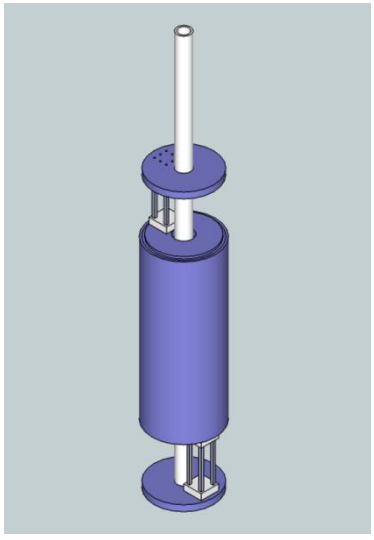

Figure 4.3 Sketch of submerged rotating circular cylinder with the top and bottom dummy section removed. Figure 5.5 shows a close-up picture of the force gauges.

The cylinder drive shaft was mounted to the support frame through two ball bearings; one at the centre of each of the two steel plates. The motor controlling the cylinder rotation was placed next to the cylinder drive shaft between the two steel plates of the support frame. The motor gearing was adjusted to give a rotational speed of the motor drive shaft between 20 rpm and 110 rpm depending on the voltage supplied to the motor. The gearbox is seen below the motor in Figure 4.2.

The gearing between the motor drive shaft and the cylinder drive shaft was 32/32 = 1, i.e. the angular position of the motor is identical to the angular position of the cylinder. This allowed the angular position of the cylinder (and the rotational speed) to be measured at the motor drive shaft with two potentiometers, see Section 5.3.

The cylinder orientation could be adjusted with the support frame as detailed in Section 4.3.1. The measuring section was made neutrally buoyant with internal buoyancy elements because of the different cylinder orientations to be tested. This prevented any gravitational loads to show up in the force time series as the cylinder rotated.

4.3.1 Cylinder Orientation

The cylinder was tested in four different orientations. Using Euler angles (where roll, pitch, and yaw (φ, θ, ψ) designates rotation around the global X-, Y-, and Z-axis respectively) the orientations can be described as θ = -5º, 0º, 5º and 10º, i.e. four different pitch angles. Figure 4.4 shows the three non-zero pitch situations. Figure 4.1 shows the situation with zero pitch.

Note that yaw corresponds to cylinder rotation. Furthermore, the flume restricts the experiments to co-linear wave and current with horizontal streamlines. Therefore, non-zero roll will, from the flows perspective, be identical to zero roll. All tests have therefore considered zero roll.

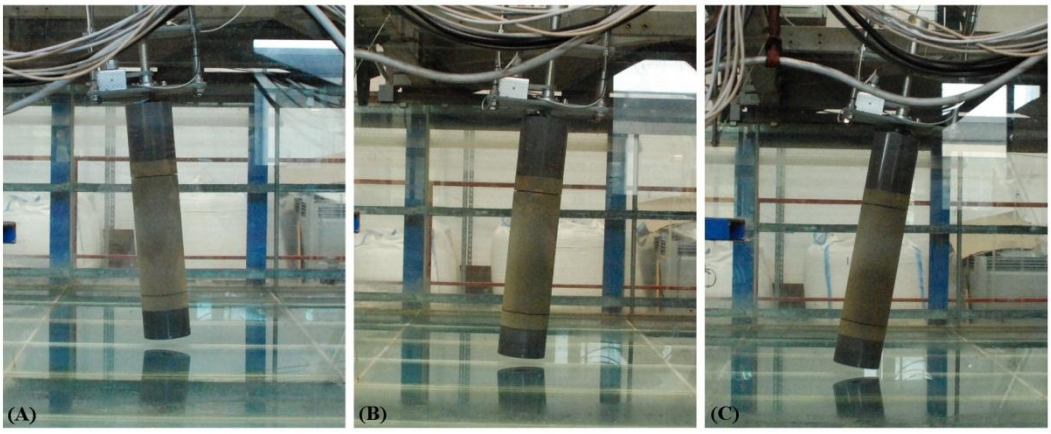

Figure 4.4 Pitch of cylinder: (a) – 5º; (b) 5º and (c) 10º. Pitch designates rotation around the global Y-coordinate.

4.3.2 Roughness

The measuring section was made rough by gluing sand, d_{50} = 0.3 mm, on to the cylinder surface. A 5 cm band, at the bottom of the top dummy section and at the top of the bottom dummy section, was also made rough. Figure 4.5 shows the grain size distribution

of the sand. Given a cylinder diameter, D = 160 mm, the relative roughness is found to be $d_{50}/D = 2 \cdot 10^{-3}$. The equivalent sand roughness, k_s, is generally found to be in the order of 1 to 3 times d_{50}. The relative roughness expressed with the equivalent sand roughness is therefore expected to be in the range $2 \cdot 10^{-3}$ to $6 \cdot 10^{-3}$.

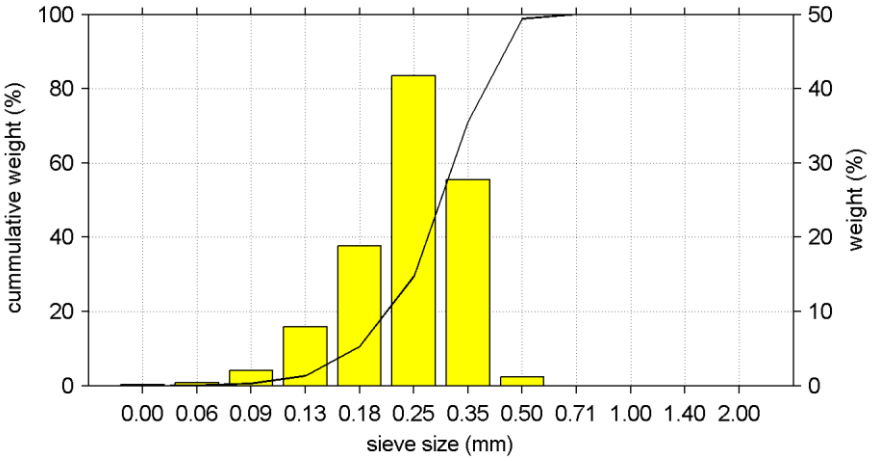

Figure 4.5 Grain size distribution of sand which was used to make the cylinder rough.

5 INSTRUMENTATION AND DATA ACQUISITION

Measurements included bulk torque, lift and drag on the cylinder. Current velocity, wave motion and rotational speed of the model were measured for reference.

5.1 Current Velocity

The current velocity measurements were carried out with a Minilab SD-12, which is an ultrasonic current meter (USCM).

The probe was mounted on the carriage and therefore measured both the carriage velocity as well as the current velocity in the flume. The probe was mounted so as to measure the current velocity at the middle of the measuring section.

5.2 Carriage Position and Velocity

The carriage position, x, along the length of the flume was measured with an SICK DT50 (P2113) laser distance measuring device.

Measurement range:	0.2 … 20 m
Resolution:	≤ 1 mm
Accuracy:	+/-7 mm

During post-processing, the position signal was low-pass filtered with a cut-off frequency of 4 Hz and differentiated with time to give the velocity of the carriage, u = dx/dt.

Figure 5.1 SICK DT50Hi (P2113) laser distance sensor

5.3 Rotational Speed and Angular Position

The angular position (rotation around the vertical, z) of the model was measured with two continuous potentiometers of type Contelec WAL305, Figure 5.2.

Measurement range:	0 … 340º (continues)
Resolution:	< 0.3º

The angular position measured was that of the motor shaft (after the motor gearbox). The motor powered the cylinder rotation through a gearing of e.g. 32/32 = 1. The angu-

lar position of the motor shaft is therefore identical to the angular position of the cylinder drive shaft.

During post-processing: (1) the two outputs were combined to achieve a 360º measurement range; and (2) a crossing-analysis of the position signal was used to determine the rotational speed. Note that differentiation of the angular position could also have given the rotational speed. This method was used to check the crossing-analysis routine.

Figure 5.2 Contelec WAL305 potentiometer

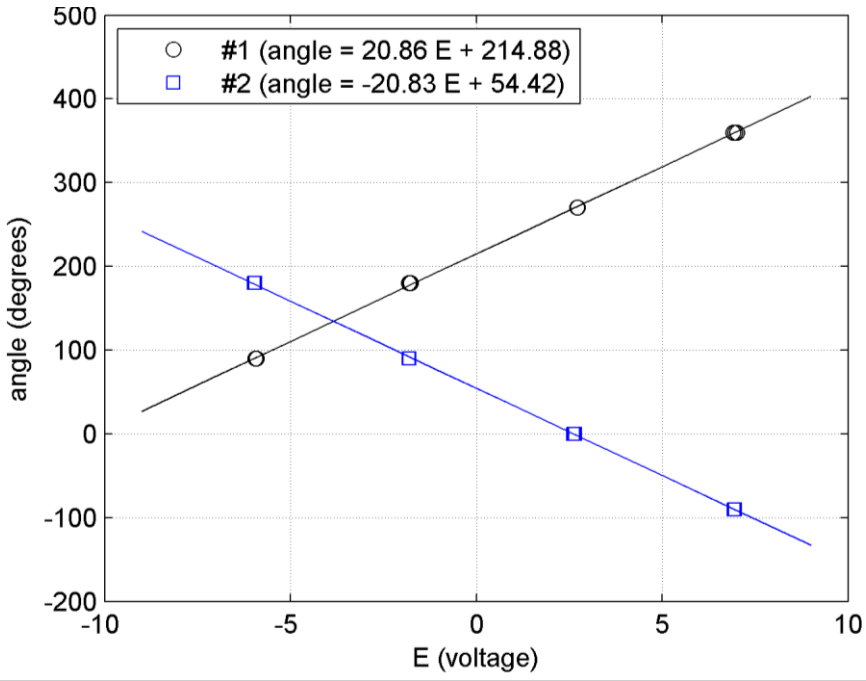

Figure 5.3 Calibration of Contelec WAL305 potentiometers.

5.4 In-line and Lift Force

The measuring section was mounted on two 2-component force gauges, see Figure 4.3. The two force gauges of type DHI-205/30, Figure 5.5, were calibrated independently and checked after assembly of the model. Figure 5.4 shows the calibration results for the two force gauges.

During post-processing the output from the two force gauges, (F_{x1}; F_{y1}) and (F_{x2}; F_{y2}), given in the local coordinate system rotating with the cylinder, was recalculated to the

global coordinate system, designated with a prime, using the angular position (yaw) of the circular cylinder, i.e.:

$$\begin{bmatrix} F'_{x1} \\ F'_{y1} \end{bmatrix} = R_z \begin{bmatrix} F_{x1} \\ F_{y1} \end{bmatrix} = \begin{bmatrix} \cos(\psi) & -\sin(\psi) \\ \sin(\psi) & \cos(\psi) \end{bmatrix} \begin{bmatrix} F_{x1} \\ F_{y1} \end{bmatrix} = \begin{bmatrix} F_{x1}\cos(\psi) - F_{y1}\sin(\psi) \\ F_{x1}\sin(\psi) + F_{y1}\cos(\psi) \end{bmatrix}$$

and similarly for the second force gauge. Here ψ is the angular position of the circular cylinder and R_z is the rotation matrix that performs the rotation. The total force in the global coordinate system is then found by:

$$F_X = F'_{x1} + F'_{x2} = (F_{x1} + F_{x2})\cos(\psi) - (F_{y1} + F_{y2})\sin(\psi)$$
$$F_Y = F'_{y1} + F'_{y2} = (F_{x1} + F_{x2})\sin(\psi) + (F_{y1} + F_{y2})cos(\psi)$$

where F_X is the resultant total in-line force and F_Y is the total cross-flow (lift) force.

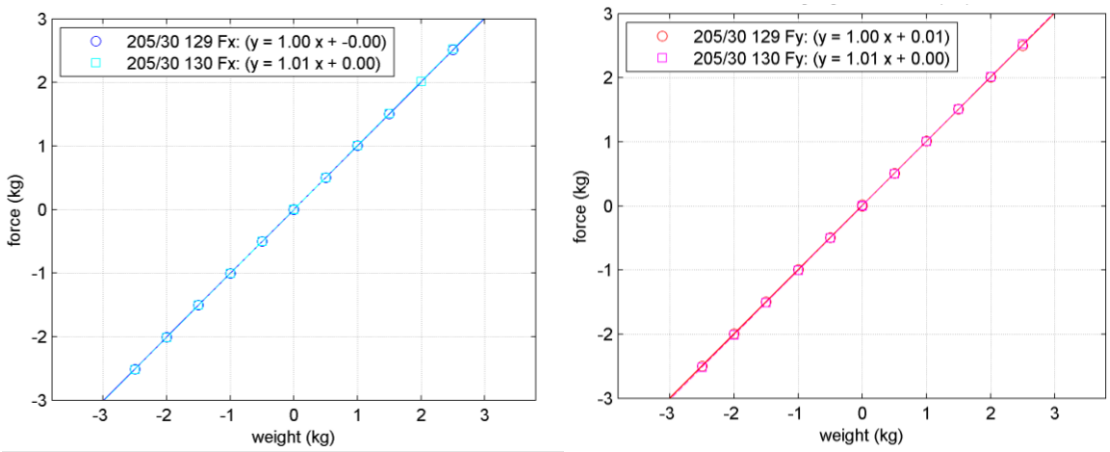

Figure 5.4 Calibration of force gauges. (Left) x-component and (right) y-component.

Figure 5.5 2-component force gauge of type DHI-205/30.

5.5 Torque

During post-processing the torque (moment) was found as follows:

$$M_z = r_1 F_{y1} - r_2 F_{y2} = r(F_{y1} - F_{y2})$$

where $r = r_1 = r_2$, and F_{y1} and F_{y2} are the angular forces measured by the two force gauges, respectively (F_{x1} and F_{x2} are the radial forces measured by the two force gauges).

5.6 Data Acquisition

Data acquisition was performed using DHI's data acquisition system, Figure 5.6.

Figure 5.6 DHI's data acquisitions system.

6 TEST CONDITIONS

All data and results are presented in model scale in this report.

6.1 Current alone

A number of validation tests were performed with steady current: the current speed was in the range U_c = 0.06 ~ 0.70 m/s. The current Reynolds number, defined:

$$Re_c = \frac{DU_c}{\nu}$$

was primarily in the subcritical range but included the lower transition: from $1 \cdot 10^4$ to $1 \cdot 10^5$. Here ν is the kinematic viscosity (0.01 $cm^2\ s^{-1}$). The water temperature was 20°C. A total of 24 tests were performed. Additional details regarding the test conditions are given in Appendix A.

6.2 Waves alone

Table 6.1 and Table A.2 (Appendix A) summarize the test conditions for wave alone tests. Note that U_m in the table is the amplitude of the free-stream velocity defined by:

$$U = U_m \sin(2\pi f t)$$

where f = 1/T is the wave frequency (T is the period of the oscillatory motion). The amplitude of the orbital motion is calculated from:

$$a = \frac{U_m T}{2\pi}$$

The Keulegan-Carpenter number and the Reynolds number, respectively are defined

$$KC = \frac{2\pi a}{D} = \frac{U_m T}{D}$$

$$Re = \frac{aU_m}{\nu} = \frac{TU_m^2}{2\pi\nu}$$

where ν is the kinematic viscosity (0.01 $cm^2\ s^{-1}$). The water temperature was 20°C.

The wave alone experiments covered KC numbers in the range 1 < KC < 24 although the majority of the tests were in the range 1 < KC < 14. A total of 42 tests were performed.

Table 6.1 Test conditions: oscillatory flow (wave) alone; Cylinder diameter, D = 160 mm

U_m	T	a	KC	Re · 10^{-4}	N
(m/s)	(s)	(m)	(-)	(-)	(-)
0.1 ~0.6	1.7 ~ 8.8		0.8 ~ 24	1.2 ~ 9.6	42

6.3 Rotation alone

A number of validation tests were performed with rotation alone: the rotational frequency was in the range $\omega/2\pi = 20 \sim 90$ rpm. Re_ω is the Reynolds number based on the surface speed:

$$Re_\omega = \frac{R(\omega R)}{\nu} = \frac{\omega R^2}{\nu}$$

was in the range $4.1 < \log_{10}(Re_\omega) < 4.8$. Here ωR is the surface speed of the cylinder. Additional details regarding the test conditions are given in Appendix A.

6.4 Current with Rotation

A number of validation tests were performed with steady current and cylinder rotation: the current speed was in the range $U_c = 0.06 \sim 0.35$ m/s; and the cylinder rotation was in the range $\omega/2\pi = 20 \sim 80$ rpm. The current Reynolds number was in the subcritical range: $1 \cdot 10^4 \sim 6 \cdot 10^4$; and the speed ratio, $\omega R/U_c$ was between 0 and 6. Additional details regarding the test conditions are given in Appendix A.

6.5 Wave with Rotation

Table 6.2 summarizes the test conditions for wave with rotation experiments.

The cylinder rotation may be expressed as the ratio of surface speed and the free stream velocity (the speed ratio):

$$\alpha = \frac{\omega D}{2U_m} = \frac{\omega R}{U_m}$$

Here R is the cylinder radius and ω is the angular frequency of the cylinder. In Table 6.2 the range of angular frequency tested has been indicated.

A total of 67 tests were performed. Additional details regarding the test conditions are given in Appendix A.

Table 6.2 Test conditions: oscillatory flow with cylinder rotation; Cylinder diameter, D = 160 mm

Wave No.	U_m	T	a	KC	Re	ω/2π	N
(-)	(m/s)	(s)	(m)	(-)	(-)	(rpm)	(-)
W01	0.13	1.74	0.03	1.4	$2.1 \cdot 10^4$	31 – 93	9
W02	0.20	1.74	0.07	2.2	$3.2 \cdot 10^4$	30 ~ 95	6
W03	0.23	3.00	0.16	4.3	$3.6 \cdot 10^4$	30 ~ 77	4
W04	0.26	2.14	0.14	3.4	$4.1 \cdot 10^4$	29 ~ 75	4
W05	0.28	2.47	0.19	4.3	$4.4 \cdot 10^4$	29 ~ 74	5
W06	0.32	2.14	0.22	4.3	$5.1 \cdot 10^4$	28	1
W07	0.39	1.74	0.26	4.2	$6.2 \cdot 10^4$	19 ~ 71	5
W08	0.44	4.55	0.32	12.5	$7.0 \cdot 10^4$	64	1
W09	0.44	5.15	0.36	14.1	$7.0 \cdot 10^4$	22 ~ 78	4
W10	0.44	5.76	0.40	15.8	$7.0 \cdot 10^4$	62	1
W11	0.44	6.36	0.44	17.4	$7.0 \cdot 10^4$	22 ~ 76	4
W12	0.44	6.97	0.49	19.1	$7.0 \cdot 10^4$	62	1
W13	0.44	7.57	0.53	20.8	$7.0 \cdot 10^4$	30 ~ 76	4
W14	0.44	8.20	0.57	22.4	$7.0 \cdot 10^4$	62	1
W15	0.44	8.80	0.61	24.1	$7.0 \cdot 10^4$	23 ~ 77	4
W16	0.46	2.14	0.46	6.2	$7.4 \cdot 10^4$	19 ~ 69	5
W17	0.50	4.02	0.98	12.4	$7.9 \cdot 10^4$	65	1
W18	0.53	2.47	0.69	8.2	$8.5 \cdot 10^4$	26 ~ 69	5
W19	0.56	4.02	1.25	14.0	$8.9 \cdot 10^4$	62	1
W20	0.62	4.02	1.54	15.6	$9.9 \cdot 10^4$	60	1

6.6 Combined Wave and Current with Rotation

Table 6.3 summarizes the test conditions for combined wave and current with rotation experiments. A total of 132 tests were performed. Additional details regarding the test conditions are given in Appendix A.

Table 6.3 Test conditions: combined wave and current with cylinder rotation; Cylinder diameter, D = 160 mm

U_m	T	a	KC	U_c	$Re_c \cdot 10^{-4}$	$\omega/2\pi$	$\omega R/(U_m+U_c)$	N
(m/s)	(s)	(m)	(-)	(m/s)	(-)	(rpm)	(-)	(-)
0.13	1.74	0.04	1.4	0.03 ~ 0.34	0.5 ~5.5	27 – 80	0.5 ~ 4.0	18
0.21	1.74	0.06	2.2	0.02 ~ 0.35	0.4 ~5.6	26 ~ 79	0.4 ~ 2.8	17
0.32	1.74	0.09	3.4	0.03 ~0.35	0.4 ~5.6	24 ~73	0.3 ~ 1.6	15
0.11	2.14	0.04	1.5	0.34	5.4	78	1.5	1
0.26	2.14	0.09	3.5	0.03 ~ 0.35	0.4 ~ 5.6	25 ~ 76	0.4 ~ 2.1	17
0.32	2.14	0.11	4.3	0.03 ~ 0.35	0.5 ~ 5.7	24 ~ 73	0.3 ~ 1.7	15
0.10	2.47	0.04	1.5	0.34	5.4	77	1.5	1
0.28	2.47	0.11	4.3	0.03 ~ 0.35	0.4 ~ 5.6	24 ~ 75	0.4 ~ 1.8	15
0.38	2.47	0.15	5.8	0.03 ~ 0.36	0.4 ~ 5.7	24 ~ 72	0.3 ~ 1.3	13
0.08	3.00	0.04	1.5	0.34	5.4	73	1.5	1
0.23	3.00	0.11	4.4	0.03 ~ 0.35	0.4 ~ 5.6	24 ~ 77	0.4 ~ 2.2	17
0.34	3.00	0.16	6.4	0.36	5.7	43	0.5	1
0.29	3.60	0.16	6.4	0.35	5.6	60	0.8	1

7 DATA ANALYSIS AND RESULTS

7.1 General

For a cylinder moved with an acceleration in still water the Morison formulation for the total in-line force reads:

$$F_X = \frac{1}{2}\rho C_D D h U|U| + \rho C_m A h \frac{dU}{dt}$$

The first term on the right-hand side is the drag force and the second term is the hydrodynamic mass force (inertia force). ρ is the water density, h is the cylinder height, D is the cylinder diameter, A is the cross-sectional area, U is velocity, C_D is the drag coefficient and C_m is the hydrodynamic mass coefficient.

7.2 Current alone

Here the acceleration term, dU/dt, in the equation for the total in-line force drops out and the total in-line force may be represented by the non-dimensional force (or force coefficient) C_D:

$$C_D = \frac{F_X/h}{\frac{1}{2}\rho D U|U|} = \frac{F_X/h}{\frac{1}{2}\rho D U_c^2}$$

Figure 7.1 shows the measured drag coefficient in the present experiments. Also shown in the figure is a general form of $C_D = C_D(Re_c, k_s/D)$ for $k_s/D = 3\cdot10^{-3}$ through $k_s/D = 9\cdot10^{-3}$ from /7/. The current alone case, which is a reference case, was extended to high Reynolds numbers although the combined rotation, wave and current tests were carried out at current Reynolds numbers in the order of 10^4. This allowed a qualitative estimate of the relative roughness expressed with the equivalent sand roughness, k_s/D, because of the branching with respect to k_s/D in the transitional regime ($RE = O(10^5)$). The qualitative estimate of the relative roughness for the present experiments is found from Figure 7.1 to be $k_s/D \approx 4\cdot10^{-3}$. This is in line with the analysis in Section 4.3.2.

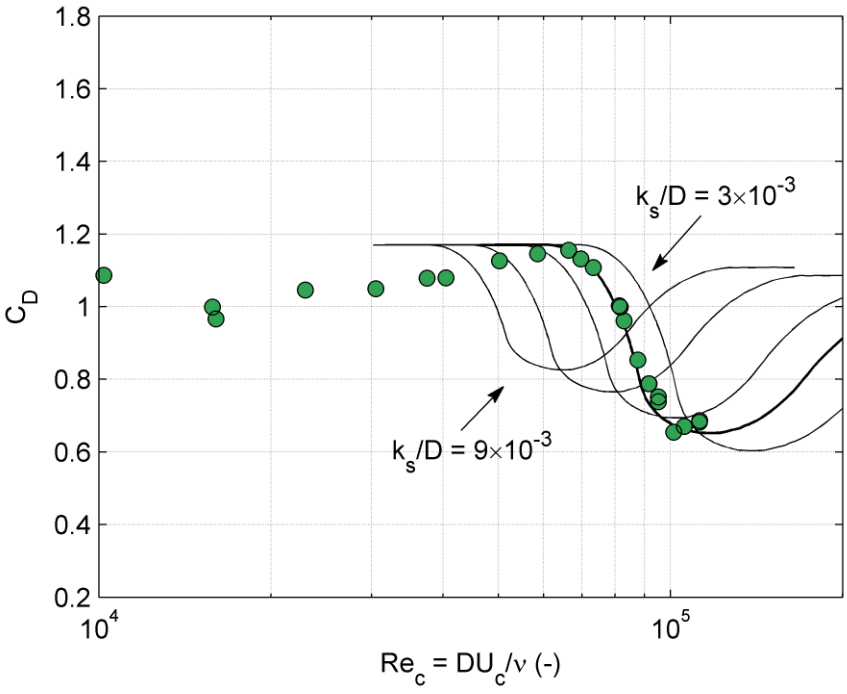

Figure 7.1 *Drag coefficient of a circular cylinder at various surface roughness parameters, k_s/D, as a function of the Reynolds number. Filled circles: present data; Curves: general form of $C_D = C_D(Re_c, k_s/D)$ curve for a rough cylinder (Basu (1985) /7/) for $k_s/D = 3\cdot10^{-3}$, $4\cdot10^{-3}$, $5\cdot10^{-3}$, $7\cdot10^{-3}$ and $9\cdot10^{-3}$.*

7.3 Wave alone

The drag coefficient, C_D, and the hydrodynamic mass coefficient, C_m, have been determined for each of the tests with waves alone as described below. The technique used for determining the force coefficients was the *method of least squares* (see /5, page 140/). The principle idea of this method is that the force coefficients are determined in such a way that the mean-squared value between the predicted force (by the Morison formula) and the measured force is minimal. Figure 7.2 shows an example of the comparison of the measured in-line force and the predicted in-line force, and Figure 7.3 shows the measured variation of C_D and C_m with the KC number.

The measuring section was made neutrally buoyant with internal buoyancy elements because of the different cylinder orientations to be tested as detailed in Section 4.3. This means that the inertia force includes a contribution from the mass of the cylinder:

$$\rho C_m' Ah \frac{dU}{dt} = \rho C_m Ah \frac{dU}{dt} + \rho Ah \frac{dU}{dt}$$

$$C_m' = C_m + 1$$

where the last term on the right-hand side is the mass of the cylinder (not to be confused with the Froude-Krylov force). The hydrodynamic force coefficient, C_m (presented in Figure 7.3) has therefore been determined from the inertia coefficient, C_m', using the above relationship: $C_m = C_m' - 1$.

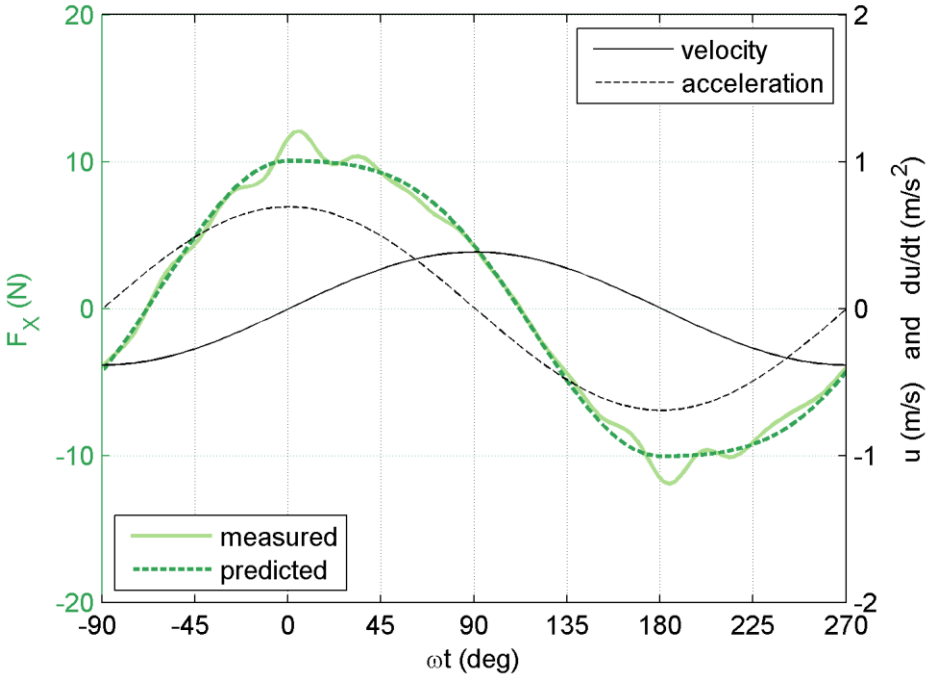

Figure 7.2 *Comparison of measured in-line force and predicted in-line force using the Morison formulation (left axis). Also shown is the velocity and acceleration (right axis). Test No. 458, KC = 8.4, C_D = 0.9, C_m = 0.8, Re = 6.2·10^4.*

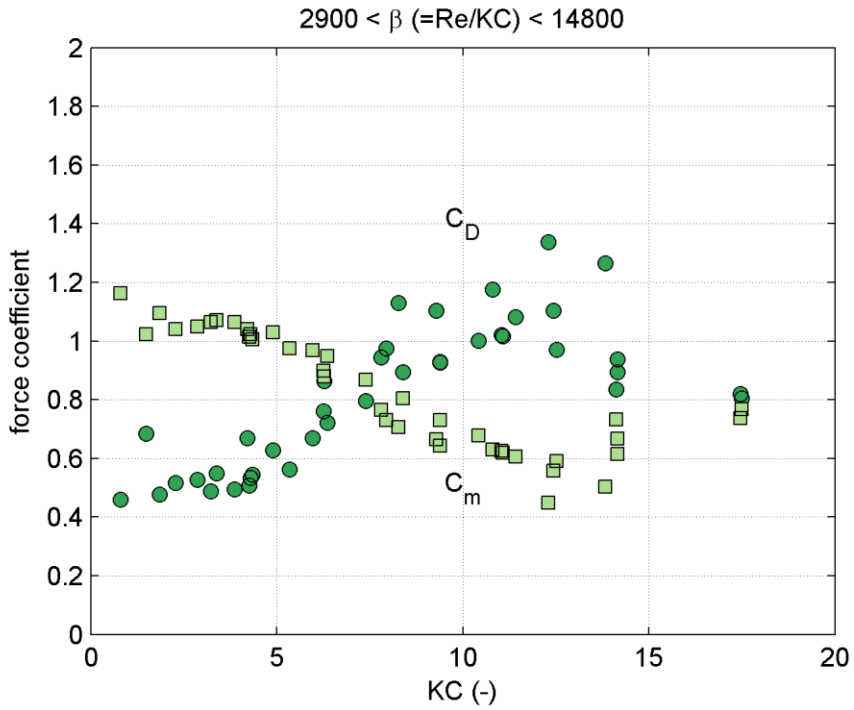

Figure 7.3 *Variation of C_D and C_m with the KC number.*

7.4 Rotation alone

The torque, M_z (moment) was measured as detailed in Section 5.5. The moment may be represented by the non-dimensional friction coefficient:

$$C_f = \frac{M_Z}{\frac{1}{2}\rho SR(\omega R)^2}$$

where S (=2πRh) is the surface area of the cylinder, ωR is the surface speed of the cylinder, and the quantity $\frac{1}{2}\rho(\omega R)^2$ is the dynamic pressure associated with the surface speed.

Figure 7.4 shows the measured friction coefficient as a function of Re_ω. Recall that Re_ω is the Reynolds number based on the surface speed:

$$Re_\omega = \frac{\omega R^2}{\nu}$$

Also plotted in the figure are data from Theodorsen & Kegier (1945) /6/. Generally, the at present measured drag coefficients are of the same order of magnitude as those reported by Theodorsen & Kegier – although slightly smaller assuming that the present relative roughness, d_{50}/R, corresponds to the relative roughness, ε/R, reported by Theodorsen & Kegier).

Theodorsen & Kegier (1945) /6/ give the relative roughness as ε/R, where ε is the *size of the sand grain*. Theodorsen & Kegier describe the sand grain as having a certain mesh size (e.g. 40 mesh) which is somewhat ambiguous. However, the mesh designation together with the reported relative grain size and the cylinder diameter, see Table 7.1 and Appendix B, suggest the sand glued to the cylinder surface by Theodorsen & Kegier to roughen the surface of the cylinder was of fairly uniform size. Theodorsen & Kegier also reported that the particle unit density was an important parameter with respect to the measured friction coefficient in the rough turbulent regime. The drag coefficient remains approximately constant under saturated conditions in this regime. In non-saturated conditions the drag coefficient falls between this limit state and the lower limit given by the smooth surface turbulent flow. The drag coefficients reproduced from Theodorsen & Kegier and given in Figure 7.4 are for a sand unit density corresponding to saturated conditions.

The above discussion indicates that the discrepancies between the present results and those presented by Theodorsen & Kegier (1945) /6/ can be related to the differences in roughness conditions. Another aspect here is the ratio R/δ, where δ is the boundary layer thickness. In other flows, such as pipe flow, this ratio is found to play a role. The cylinder diameter is practically identical in the two studies, however, difference in medium, i.e. water versus air, means that the ratio, R/δ, may be as much as a factor of 4 smaller in the experiments performed and reported by Theodorsen & Kegier than the present study.

All things considered it seems that it is possible to measure drag coefficient (moment forces) although the experimental setup also has to handle much larger forces such as the Magnus effect and inertia forces. The smaller the rotational frequency the more dif-

ficult it naturally becomes to accurately measure the friction coefficient with the present setup. This may explain why two data points, the two data points with the lowest rotational speeds tested, fall below the line for smooth wall, turbulent boundary layer flow. These small rotational speeds have therefore been disregarded when determining the torque in the following sections.

Table 7.1 Information extracted from legend of Figure 8 in Theodorsen & Kegier (1945) /6/. First four columns are directly copied from legend. From this information the last two columns have been calculated assuming that 1 inch equals 25.4 mm.

Symbol	ε/R	D	Sand	R	ε
		(in)		(mm)	(mm)
o	0.06	½	40 mesh	6,35	0,381
+	0.03	1	40 mesh	12,7	0,381
x	0.012	1	100 mesh	12,7	0,152
^	0.005	6	40 mesh	76,2	0,381
v	0.002	6	100 mesh	76,2	0,152

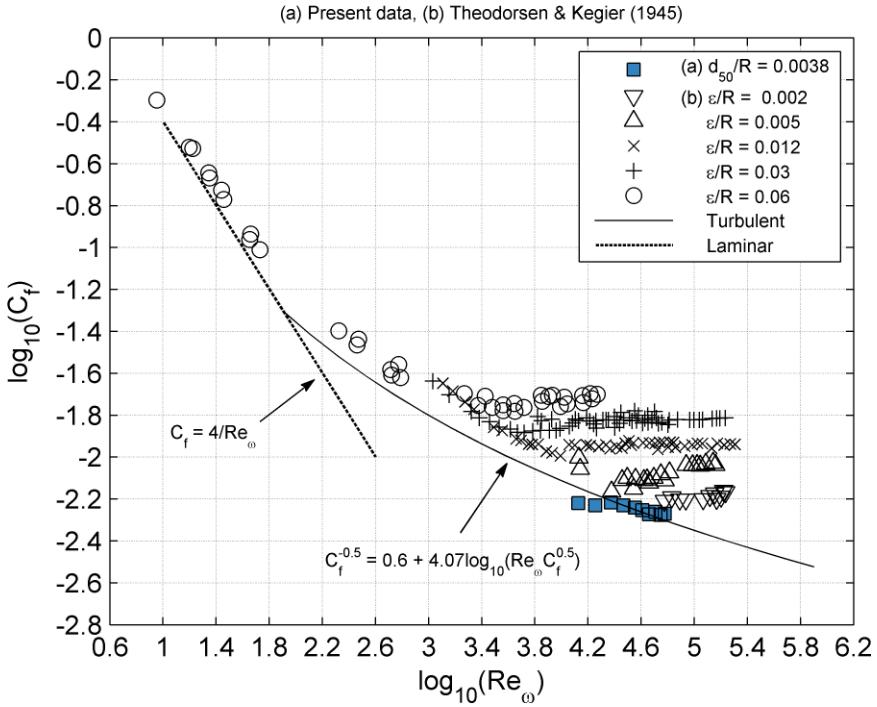

Figure 7.4 Friction coefficient, C_f, as a function of Re_ω. (a) Solid squares: present data; (b) Other data from Theodorsen & Kegier (1945) /6/. Dotted line: smooth surface, laminar flow. Solid line: Smooth surface, turbulent flow.

7.5 Current with Rotation

For clock-wise rotating circular cylinder in steady flow (see sketch in Figure 7.5), the velocity of the upper surface of the cylinder is in the same direction as the free-stream velocity. Separation is thereby delayed on the upper surface, while it occurs earlier on the lower surface. Thus the pressure distribution on the cylinder surface is altered when the rotation is present. Pressure is reduced on the upper surface and increased on the lower surface, causing a positive net lift force. This effect is known as the *Magnus ef-*

fect. Rotation in the opposite direction reverses this effect and causes a negative lift force. The lift force can be represented by a non-dimensional lift force (or lift coefficient):

$$C_L = \frac{F_Y/h}{\frac{1}{2}\rho D U|U|}$$

and the mean drag coefficient (in-line force) is determined as for the current alone case. Figure 7.5 shows the measured lift and drag coefficient as a function of the speed ratio, $\omega R/U_c$, the ratio of surface speed to free-stream flow speed. In Figure 7.5 experimentally measured lift and drag coefficient for Reynolds numbers between 40 000 and 660 000 from /3/ has also been included. The present data are in good agreement with the data from /3/.

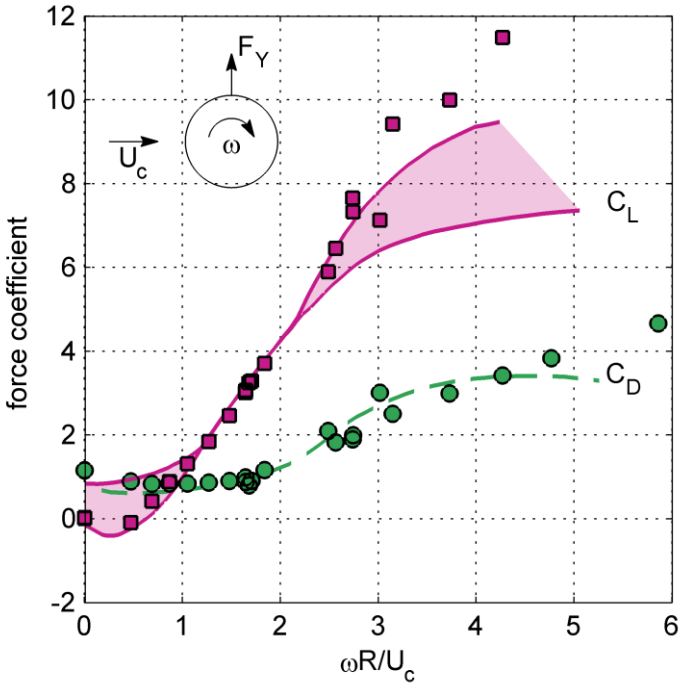

Figure 7.5 Lift and drag of a rotating cylinder as a function of speed ratio: Magnus force. Circles and squares: present data; lines: /3/.

The data band reported by /3/ for the lift coefficient is attributed to the range of Reynolds numbers. Specifically the negative lift is reported to occur for small speed ratios in the critical Reynolds number range of 10^5 to $5 \cdot 10^5$. The present results are obtained for a rough cylinder. Cylinder roughness has the effect of reducing the critical Reynolds number (/4/). Because of the lack of information about roughness conditions, and the reported critical Reynolds number, it is concluded that the data reported by /3/ are for smooth cylinders. This may explain why the present results indicate a negative lift for small spin ratios although the current Reynolds numbers are smaller than those listed by /3/. Note the highest current Reynolds number in the present experiments will be associated with the smaller speed ratios.

For subcritical Reynolds numbers the drag coefficient takes the value obtained in the case of smooth cylinders irrespective of cylinder roughness (/4/). Generally, the current Reynolds numbers are in the subcritical regime and a good comparison between the present data and the drag coefficient reported by /3/ is observed.

Potential flow theory predicts zero drag force ($C_D = 0$) and a lift force given by:

$$F_Y/h = \rho\Gamma U_c = \rho(2\pi\omega R^2)U_c$$

the *Kutta-Joukowski theorem*. Hence, potential flow theory predicts a lift coefficient given by:

$$C_L = \frac{\rho(2\pi\omega R^2)U_c}{\rho R U_c^2} = 2\pi\frac{\omega R}{U_c} = 2\pi\alpha$$

This theoretical value is much higher than experimental results suggest (Figure 7.5), a discrepancy that is primarily due to viscosity. However, the measured variation of C_L with respect to the spin ratio is to some extent in accordance with the theoretically predicted linear variation – at least over a certain range of speed ratios.

7.6 Wave with Rotation

Figure 7.6 gives the definition sketch for oscillatory flow (wave) with cylinder rotation. In the following, first, the potential flow solution is considered, secondly, the cross-flow force will be considered and subsequently the attention will be directed to the in-line force and the friction torque.

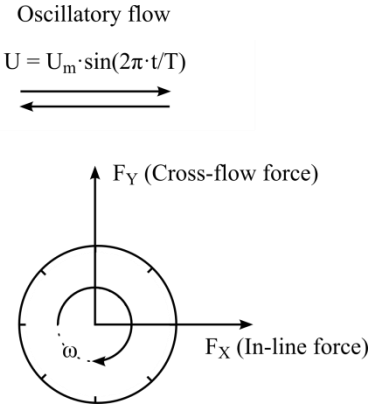

Figure 7.6 Definition sketch for oscillatory flow (wave) with cylinder rotation

7.6.1 Potential Flow Theory

The potential flow solution considers an accelerated cylinder with rotation, moving with velocity, U, in an otherwise still fluid, rather than having the cylinder held stationary (with rotation) and the fluid moves with a velocity, U, in the negative direction of the X-axis. This is similar to how the experiments have been performed.

The flow field introduced by accelerating a circular cylinder with rotation through a fluid can be calculated using potential flow theory if frictional effects are neglected (see Appendix C); and the pressure on the cylinder surface may be written as:

$$\frac{p}{\rho} = -\rho\frac{\Gamma U}{\pi R}sin\theta - \rho R\frac{dU}{dt}cos\theta + \rho U^2\cos(2\theta) + \text{constant}$$

The resultant force can be calculated by integrating the pressure around the cylinder:

$$\frac{F_X}{h} = -\int_0^{2\pi} pcos(\theta)(Rd\theta) = \rho\pi R^2\frac{\partial U}{\partial t}$$

$$\frac{F_Y}{h} = -\int_0^{2\pi} pcos(\theta)(Rd\theta) = \rho\Gamma U = \rho(2\pi\omega R^2)U$$

where F_X is the in-line force and F_Y is the cross-flow force neglecting frictional effects. The in-line force is known as the hydrodynamic mass force when considering the wave alone case, see e.g. /5, Page 127/; while the cross-flow force is the Kutta-Joukowski law when considering steady flow around a rotating cylinder, see e.g. /9, page 90/.

7.6.2 Cross-flow Force

Frictional effects may, as seen from the potential flow solution in the preceding section, cause the inertia component (the hydrodynamic mass force) of the pressure around the cylinder to contribute to the resulting cross-flow force.

An equation for the cross-flow force may therefore be formulated as:

$$\frac{F_Y}{h} = \rho AC_\Gamma\omega U + \rho AC_m\frac{dU}{dt}$$

where $A = \pi R^2$ and the coefficient, C_Γ, has been introduced to handle frictional effects, i.e. in potential flow, $C_\Gamma \equiv 2$.

The Kutta-Joukowski law, the first term in the equation above, may be expressed as for the current with rotation case (Section 7.2), i.e.:

$$\rho AC_\Gamma\omega U \equiv \frac{1}{2}\rho C_L DU|U|$$

From this it is found that C_Γ can be described by:

$$C_\Gamma = \frac{C_L}{\pi}\frac{|U|}{\omega R} \quad \leftrightarrow \quad C_L = \pi C_\Gamma\frac{\omega R}{|U|}$$

Inserted into the formulation for the cross-flow force gives:

$$\frac{F_Y}{h} = \frac{1}{2}\rho C_L DU|U| + \rho AC_m\frac{dU}{dt}$$

The lift coefficient, C_L (or the Kutta-Joukowski coefficient) and the hydrodynamic mass coefficient, C_m, can therefore be determined using the *method of least squares*. It is,

however, important which formulation for the cross-flow force is used in the method of least squares. The formulation with C_Γ assumes that the cross-flow force is a function of the velocity, U, with a small correction for the hydrodynamic mass; while the formulation with C_L assumes that the cross-flow force is a function of the velocity squared, U|U|.

Figure 7.7 shows the ensemble-averaged cross-flow force at different KC numbers. Also included in the graphs are the measured velocity and acceleration. The graphs show that the cross-flow force variation is similar to the velocity for KC < 10; while F_Y is proportional to the velocity squared, U|U| for KC > 10. There is in both cases a small phase shift between the velocity and the cross-flow force indicating a contribution from inertia as argued for at the beginning of this section.

The test conditions (Section 6.5) show that there are no tests with a KC number in the range 8.2 < KC < 12.5. The change from one flow regime to the other may therefore occur anywhere in the range 8.2 < KC < 12.5 and the limit KC ≡ 10 between the two regimes should therefore be regarded as a best guess based on the present data. Interestingly the KC number range, 8.2 < KC < 12.5, coincides with the transverse vortex-street regime (7 < KC < 13) and the start of vortex shedding (KC > 7) in pure oscillatory flow around a non-rotating cylinder, see /5/. Vortex shedding is therefore the most likely cause for the change in flow regime in oscillatory flow about a rotating cylinder.

The lift (or Kutta-Joukowski) and inertia coefficient has been determined using the method of least squares:

For **KC < 10** the formulation with C_Γ has been used. Figure 7.8 shows the lift, expressed with C_Γ and C_m, as a function of the relative rotational speed. C_Γ is in the order of 1 when $\omega R/U_m = 0.5$. It gradually decreases with increasing speed ratio and appears to approach the value 0.4 asymptotically for $\omega R/U_m > 4$. A value that is substantially smaller than the potential flow solution, $C_\Gamma \equiv 2$. Even at small speed ratios, such a $\omega R/U_m = 0.5$, the measured C_Γ is only half of the value predicted by the potential flow solution. For $\omega R/U_m < 0.5$ the Kutta-Joukowski coefficient is expected to increase with decreasing speed ratio, although with an upper limit given by the potential flow solution, $C_\Gamma \equiv 2$. The inertia coefficient, C_m, appears to attain a constant value of 0.2 over the entire range of speed ratios tested ($0.5 < \omega R/U_m < 6$), if the scatter in the data points is neglected. Figure 7.7 includes the predicted cross-flow force. The predicted cross-flow force is calculated from the determined force coefficients using the cross-flow force formulation. The figure shows a good agreement between the measured and predicted cross-flow force. There are, however, some soft fluctuations in the measured cross-flow force that are not captured by the proposed formulation. If such fluctuations are located around the phase of maximum acceleration ($\omega t = 0$ and $\omega t = 180$) it may have a large impact on the determined inertia coefficient and may explain the scatter in the data point observed for C_m.

For **KC > 10** the formulation with C_L has been used. Figure 7.10 shows the lift as a function of the relative rotational speed. The number of data points with KC > 10 is limited. However, the lift coefficient, C_L, shows a clear trend to increase with the relative rotational speed; while the inertia coefficient again scatters around the value 0.2.

The Kutta-Jouwski coefficient, C_Γ, (Figure 7.8) has been recalculated to a lift coefficient, C_L. The corresponding lift coefficient is shown in Figure 7.9. The lift coefficient

is, as for KC > 10, a function of the relative rotational speed. Indeed the data points for KC < 10 and KC > 10 coincide. This may, however, not be the case for larger relative rotational speeds. From Figure 7.9 it is seen that the lift coefficient, $C_L \approx 4$, at a speed ratio, $\omega R/U_m = 2$, for oscillatory flow around a rotating cylinder. This is the same value as for steady flow around a rotating cylinder. For $\omega R/U_m < 2$ the lift coefficient in the unsteady case is higher than in the steady case. And for $\omega R/U_m > 2$ the lift coefficient is smaller in the unsteady case than in the steady case. In the steady case for an ideal fluid, $\omega R/U_c = 2$, corresponds to the instance when the two stagnation points coincide to form a single stagnation point at the bottom of the cylinder surface. Above this value the single stagnation point will move off into the fluid as either a single stagnation point or two stagnation points. This may possibly be related to the observed difference between the unsteady and steady case.

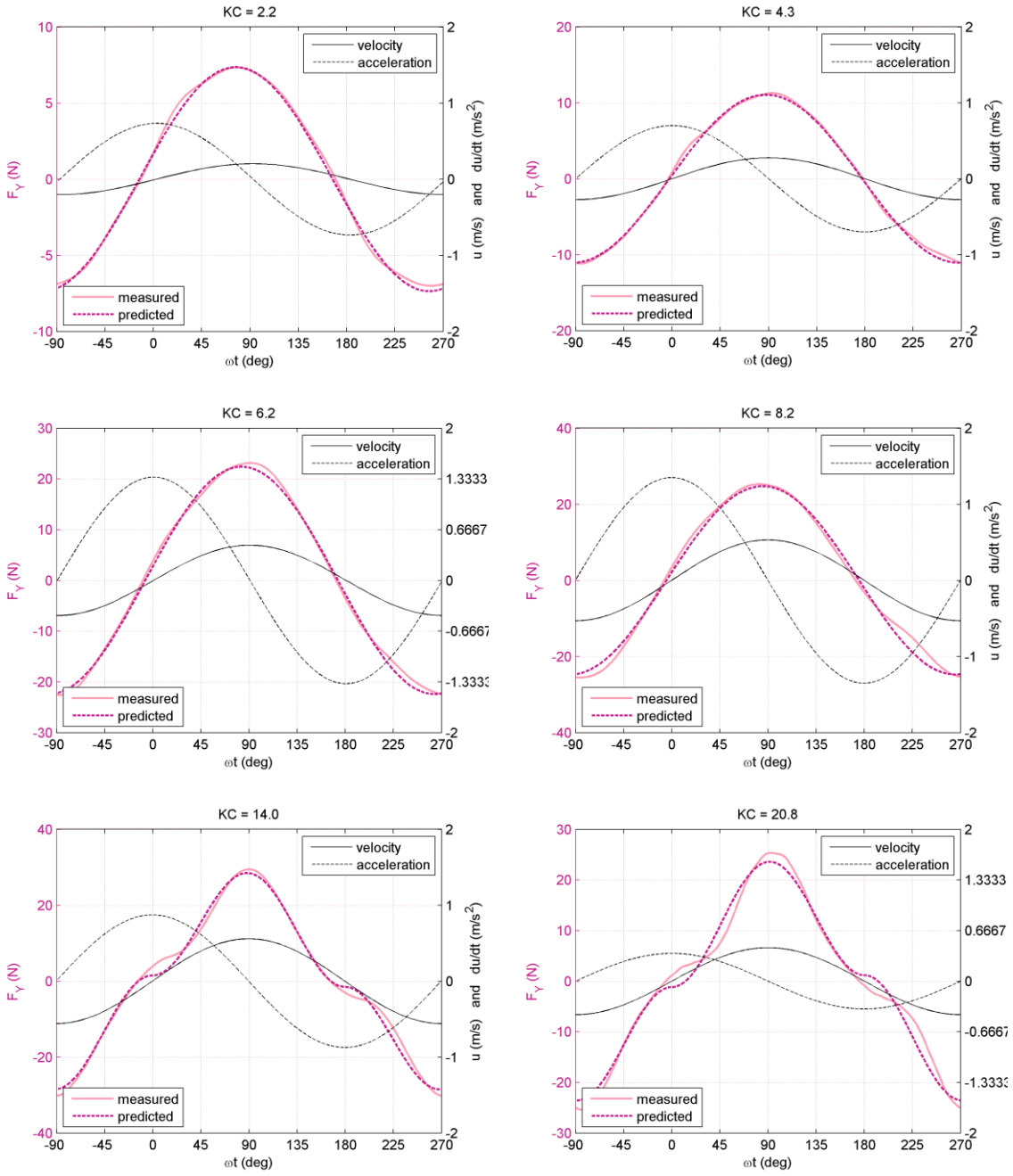

Figure 7.7 *Comparison of measured and predicted cross-flow force: (a) KC = 2.2, (b) KC = 4.3, (c) KC = 6.2, (d) KC = 8.2, (e) KC = 14.0, (f) KC = 20.8. Test No. 165, 153, 169, 131, 1023, 988, respectively.*

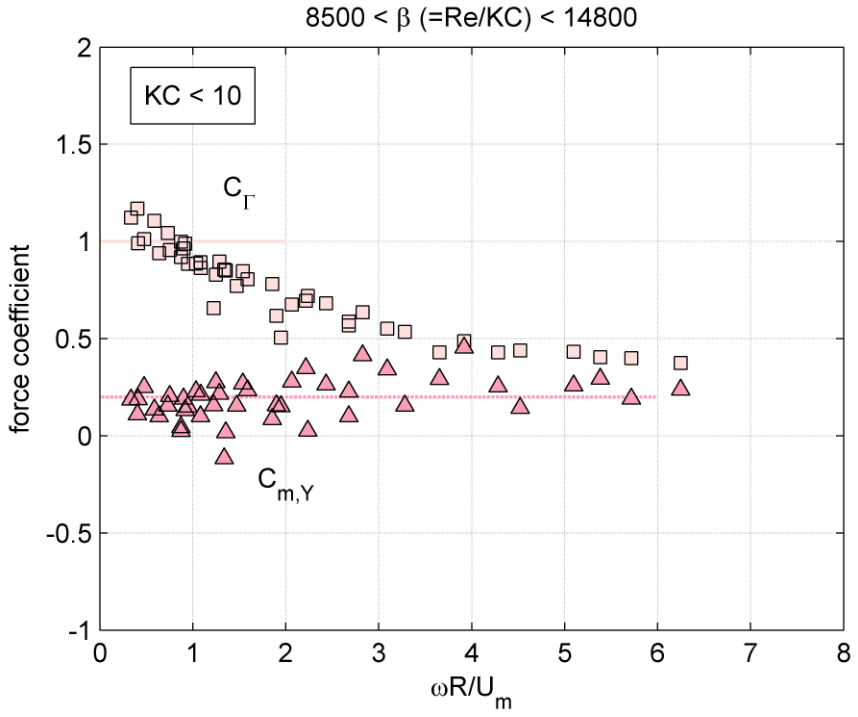

Figure 7.8 Lift, expressed with C_Γ and C_m, of a rotating cylinder in waves as a function of relative rotational speed (KC < 10).

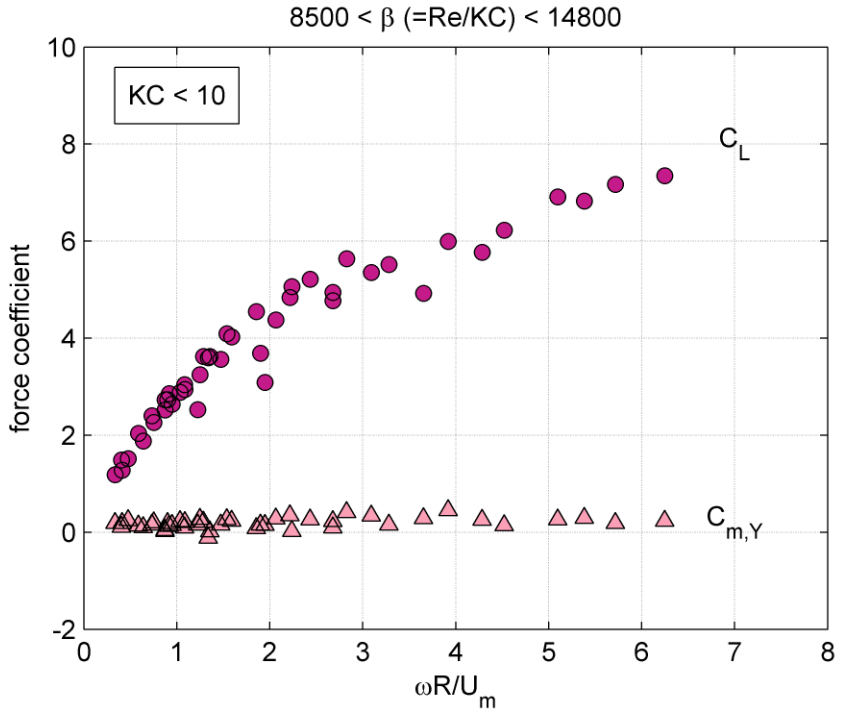

Figure 7.9 Lift of a rotating cylinder in waves as a function of relative rotational speed (KC < 10).

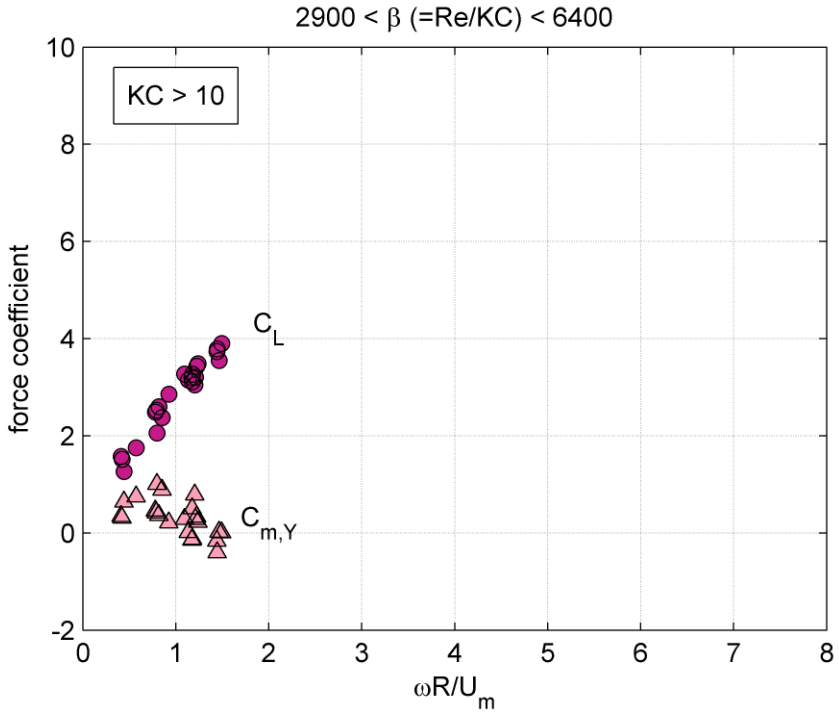

Figure 7.10 Lift of a rotating cylinder in waves as a function of relative rotational speed (KC > 10).

7.6.3 Torque

The average friction torque, M_z (moment) was calculated as detailed in Section 5.5. The moment may be represented by the non-dimensional friction coefficient as detailed in Section 7.4. Figure 7.11 shows the measured friction coefficient as a function of Re_{ω}. Also plotted in the figure are data from Theodorsen & Kegier (1945) /6/. Generally, the drag coefficients for the wave with rotation case are of the same order of magnitude as those for rotation alone.

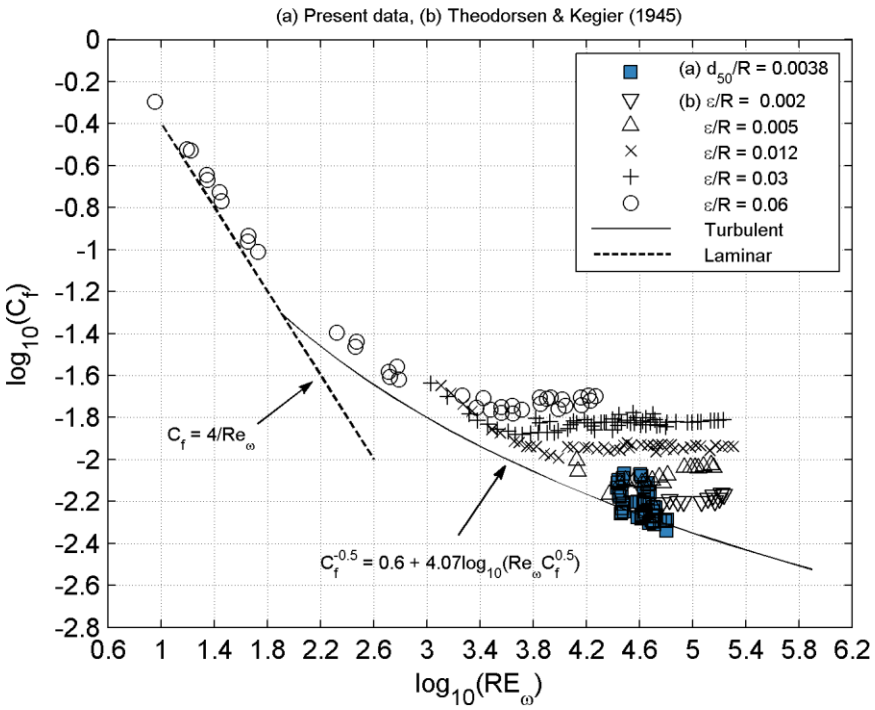

Figure 7.11 Friction coefficient, C_f, as a function of Re_ω. (a) Solid squares: present data; (b) Other data from Theodorsen & Kegier (1945) /6/. Dotted line: smooth surface, laminar flow. Solid line: smooth surface, turbulent flow.

7.6.4 In-line Force

The in-line force is determined as for the wave alone case, see Section 7.3. Figure 7.12 shows the measured in-line force expressed as a drag and inertia coefficient (hydrodynamic mass coefficient). Only data point for KC < 10 has been shown. The results suggest little difference as compared to the wave alone case, although the scatter in the data points is larger. Particularly, the drag coefficient for KC < 5 (inertia dominated) shows large scatter. This is, however, to be expected as small phase lags may have a huge impact on the determined drag coefficient.

The number of data points is small for KC > 10. There is, however, an indication that the cylinder rotation, i.e. the Magnus effect, could be affecting the in-line force. No trend has, however, been established from the limited number of data points.

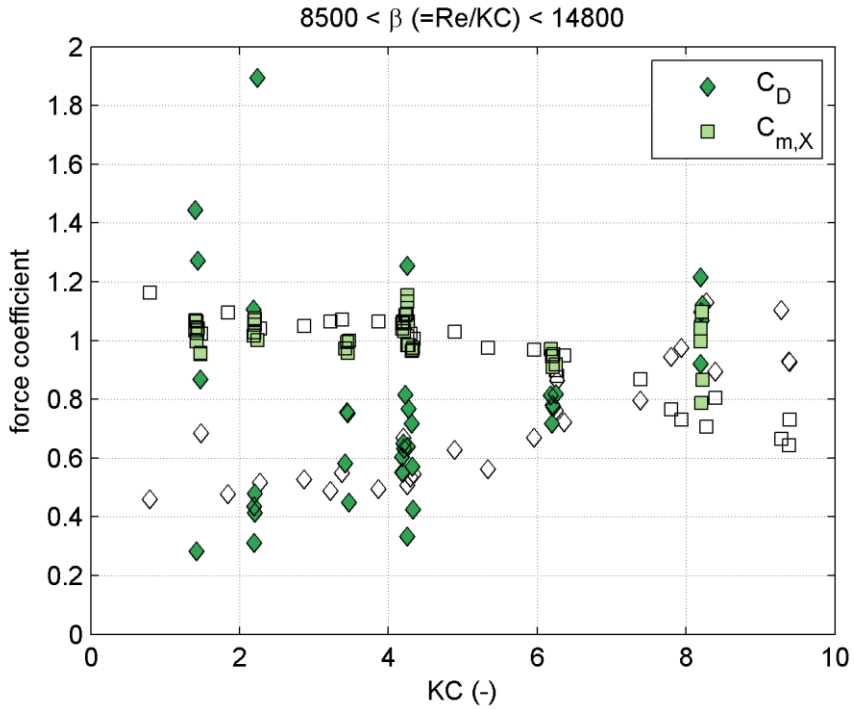

Figure 7.12 Variation of C_D and C_m with KC number for the case wave with rotation. Open symbols: wave alone, no cylinder rotation.

7.6.5 *In-line Versus Cross-flow Force*

Figure 7.13 shows the in-line force (inclusive of the Froude-Krylov force) versus the cross-flow force. The figure shows that the in-line force is generally larger than the cross-flow force for KC < 10 and vice versa when KC > 10. For KC < 10 the lift force is in the order of (0.5 to 2 times) the in-line hydrodynamic mass force (in-line force without the Froude-Krylov force); while it may be as much as a factor of 4 larger for KC > 10.

For KC < 10 the maximum in-line and cross-flow force can be written as:

$$\max\{|F_X|\} \approx \max\left\{\rho A h C_M \frac{dU}{dt}\right\} = \rho A h C_M \frac{2\pi}{T} U_m$$

$$\max\{|F_Y|\} \approx \max\{\rho A h C_\Gamma \omega U\} = \rho A h C_\Gamma \omega U_m$$

respectively, when the Froude-Krylov force has been considered in the in-line force, i.e. $C_M = C_m + 1$. Recall that ω is the angular frequency of the cylinder rotation, and f = 1/T is the wave frequency (the inverse of the wave period); and note that there is approximately a 90 degree phase difference between the maximum in-line force and the maximum cross-flow force. The ratio between the maximum cross-flow force and the maximum in-line force then reads:

$$\frac{max\{|F_Y|\}}{max\{|F_X|\}} \approx \frac{\rho A h C_\Gamma \omega U_m}{\rho A h C_M \frac{2\pi}{T} U_m} = \frac{C_\Gamma}{C_M} \frac{\omega T}{2\pi}$$

which says that if U_m and T are kept constant (which means that KC is constant and C_M is constant) then the maximum cross-flow force will increase with ω given the weak variation of C_Γ with ω (Figure 7.8 with fixed U_m). Furthermore, for small KC numbers (KC < 5) the force ratio will be a function of C_Γ when keeping ω and T constant where $C_M = 2$. Given the weak variation of C_Γ with U_m (Figure 7.8 with fixed ω) especially for ωR/Um > 2 there will be an almost constant ratio between the maximum in-line and cross-flow force. The two situations have been illustrated in Figure 7.13. Generally, the force ratio is difficult to describe with the non-dimensional parameters, KC and $\omega R/U_m$.

For KC > 10 the limited number of data points shows a linear trend. This may, however, not be the case provided that the data set is extended.

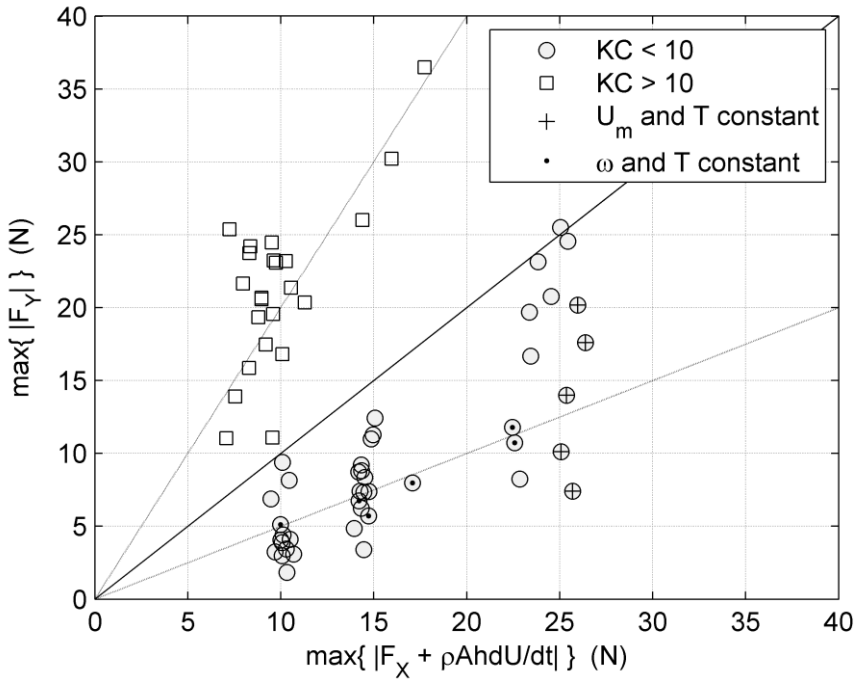

Figure 7.13 In-line (incl. Froude-Krylov force, ρAhdU/dt) versus cross-flow force for the case: wave with rotation.

7.7 Combined Waves and Current with Rotation

Figure 7.14 gives the definition sketch for combined oscillatory flow and current with cylinder rotation. In the following, first, the cross-flow force will be considered and subsequently the attention will be directed to the in-line force.

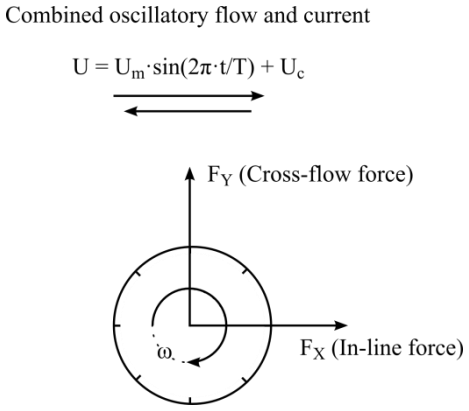

Figure 7.14 Definition sketch for combined oscillatory flow and current with cylinder rotation

7.7.1 Cross-flow Force

The cross-flow force is determined as for the wave with rotation case (Section 7.6.2). The test conditions cover KC < 10; current speed of up to 0.35 m/s which resulted in a relative strength of the wave to current of $0 < U_c/(U_m + U_c) < 0.8$ where $U_c/(U_m + U_c) = 0$ corresponds to wave alone and $U_c/(U_m + U_c) = 1$ is current alone. For KC < 10 the formulation for the cross-flow force, used in Section 7.6.2, reads:

$$F_Y = \rho A C_\Gamma \omega U + \rho A C_m \frac{dU}{dt}$$

where $U = U_m \cdot \sin(2\pi \cdot t/T) + U_c$ and the Kutta-Joukowski coefficient, C_Γ, may be recalculated to a lift coefficient:

$$C_\Gamma = \frac{C_L}{\pi}\frac{(U_m + U_c)}{\omega R} \quad \leftrightarrow \quad C_L = \pi C_\Gamma \frac{\omega R}{(U_m + U_c)}$$

Figure 7.15 and Figure 7.16 show the lift and inertia coefficient determined for all tests. In Figure 7.15 tests with $U_c/(U_m + U_c) < 0.5$ (*wave dominated*) are given; while $U_c/(U_m + U_c) > 0.5$ (*current dominated*) are shown in Figure 7.16. The figures show the force coefficients as a function of the ratio $\omega R/(U_m+U_c)$. Hence, the wave alone case is a special case, although not included in the figures. Indeed the force coefficient determined for the wave dominated combined wave and current with rotation coincides with the wave alone with rotation case.

The tests with current dominated flow are limited to a small range: $0 < \omega R/(U_m+U_c) < 2$ and $0.5 < U_c/(U_m + U_c) < 0.8$. In this range the lift coefficient is found to coincide with the lift coefficient found for the wave dominated case; while the cross-flow inertia coefficient appears to scatter around 0, i.e. no phase lag. This is expected as the flow is current dominated.

Figure 7.17 shows the cross-flow inertia coefficient as a function of the relative wave to current strength. For $U_c/(U_m + U_c) < 0.4$ the cross-flow inertia coefficient scatters around the value 0.2. Above $U_c/(U_m + U_c) = 0.4$ the cross-flow inertia coefficient (the phase lag) reduces while the scatter increases. This could suggest that in the current dominated regime the cross-flow inertia coefficient should be 0, i.e. that there is no phase lag.

Realistic full-scale current speeds correspond to less than 0.15 m/s in the model. In Figure 7.18 data points have been limited to test conditions with current speed less than 0.15 m/s. In this case the force coefficients coincide with those found for the wave with rotation case.

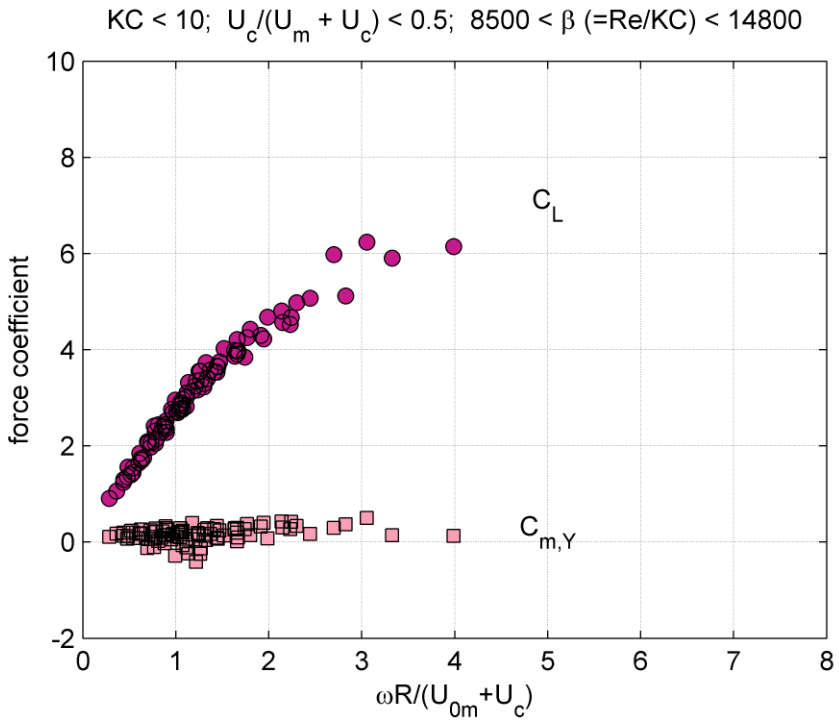

Figure 7.15 Lift of a rotating cylinder in combined wave and current as a function of the relative rotational speed. Wave dominated: $U_c/(U_m + U_c) < 0.5$ (KC < 10; 8500 < Re/KC < 14800).

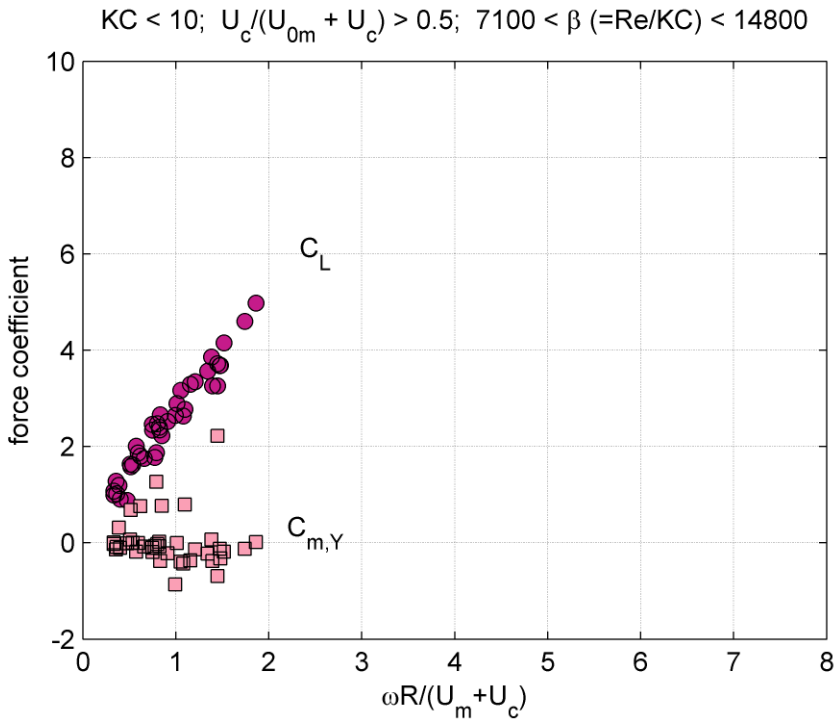

Figure 7.16 Lift of a rotating cylinder in combined wave and current as a function of the relative rotational speed. Current dominated: $U_c/(U_m + U_c) > 0.5$ ($KC < 10$; $7100 < Re/KC < 14800$).

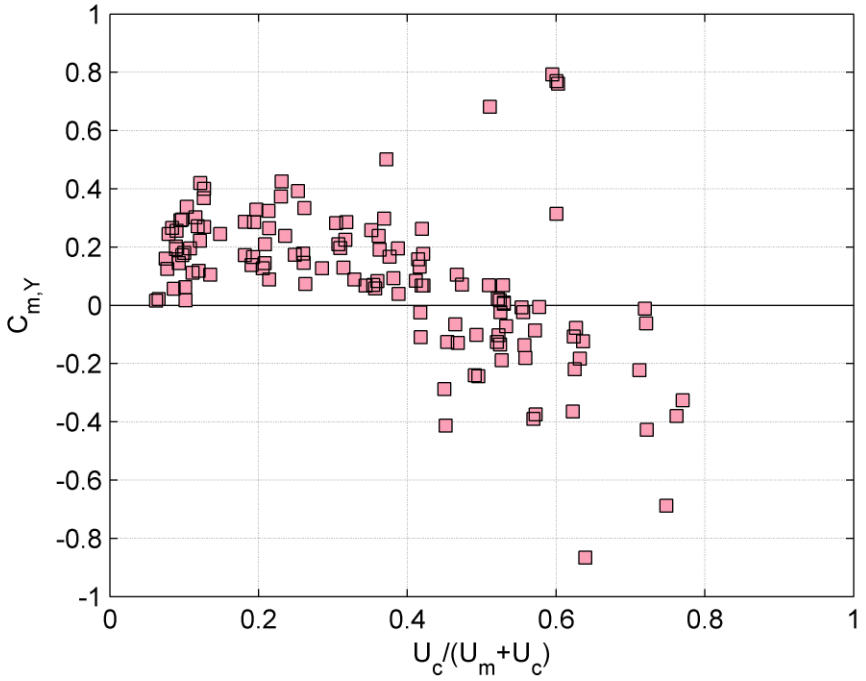

Figure 7.17 Cross-flow inertia coefficient as a function of the relative strength of the wave to current, $U_c/(U_{0m} + U_c)$. $KC < 10$. $0 < \omega R/(U_m + U_c) < 4$.

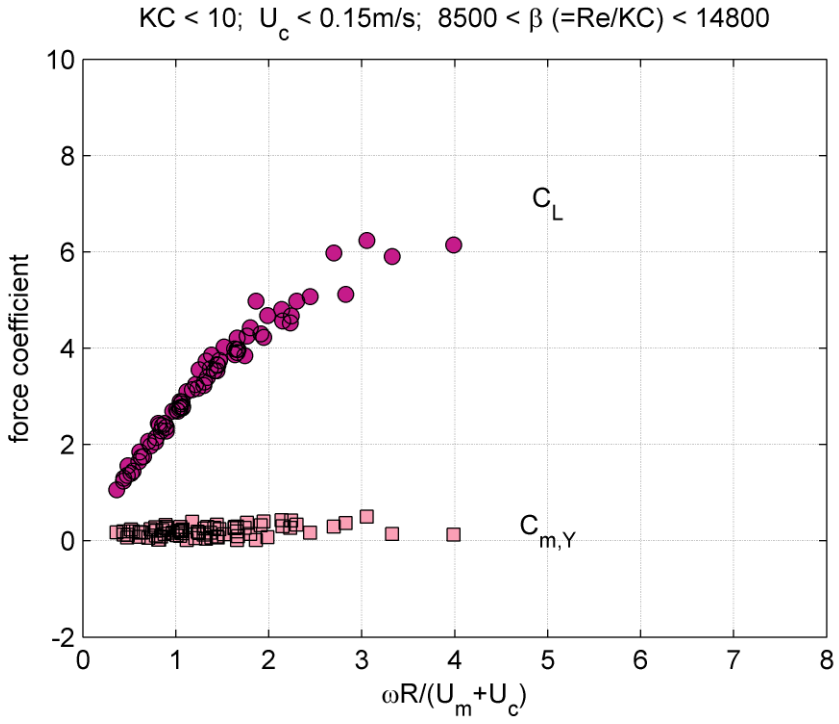

Figure 7.18 Lift of a rotating cylinder in combined wave and current as a function of the relative rotational speed. Current speed: U_c < 0.15 m/s (KC < 10, 8500 < Re/KC < 14800).

7.7.2 *In-line Force*

The in-line force is determined as for the wave alone case, see Section 7.3. The test conditions cover KC < 10; $0 < U_c/(U_m + U_c) < 0.8$ and $0 < \omega R/(U_m + U_c) < 4$. The results suggest little influence on the speed ratio for KC < 10. This was also the conclusion for the case: wave with rotation when KC was less than approximately 10. No tests were conducted with KC > 10 for the combined wave and current with rotation, but some effect of the speed ratio may be expected with increasing KC number as for the case: wave with rotation.

The effect of co-existing current on in-line forces is shown in Figure 7.19 and Figure 7.20. Figure 7.19 shows the drag component and Figure 7.20 shows the inertia component.

The *drag coefficient* scatters around the value 0.6 in the wave dominated regime ($U_c/(U_m + U_c) < 0.4$), which is in good agreement with the results for the cases: (1) wave alone and (2) wave with rotation. With increasing current component the drag coefficient increases and is expected to approach asymptotically the value(s) for the current with rotation case. In the current with rotation case (Section 7.5) the drag coefficient was found to vary with the speed ratio. The asymptotical value is therefore expected to depend on the speed ratio which also means that the drag coefficient is expected to show increasing dependency on the speed ratio with increasing $U_c/(U_m + U_c)$ in the current dominated regime. The present result, however, has a limited number of tests in the current dominated regime and the expected behaviour is not visible in the data.

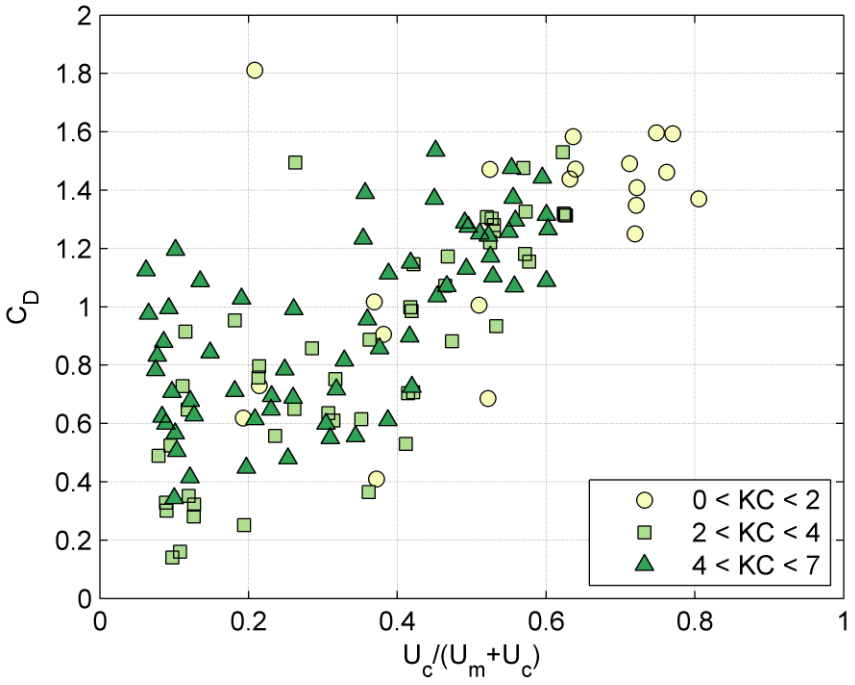

Figure 7.19 Drag coefficient as a function of the relative wave and current strength, $U_c/(U_m + U_c)$. Combined wave and current with rotation. KC < 10.

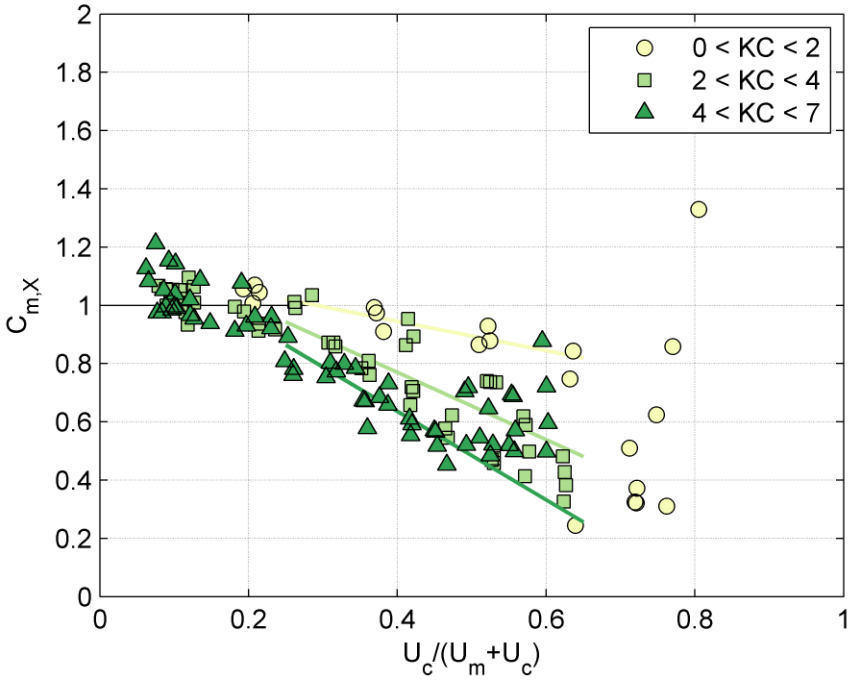

Figure 7.20 In-line inertia coefficient as a function of the relative wave to current strength, $U_c/(U_m + U_c)$. Combined wave and current with rotation. KC < 10.

The *inertia coefficient* scatters around the value 1 in the strongly wave dominated regime ($U_c/(U_m + U_c) < 0.2$) as expected. It decreases with the ratio $U_c/(U_m + U_c)$. In /6, page 158/ it is reported that the inertia coefficient is not very sensitive to U_c/U_m, except for the KC = 5 case. Interestingly this coincides with the KC numbers where the present data show sensitivity to the velocity ratio, $U_c/(U_m + U_c)$.

8 REFERENCES

/1/ L. Vita, U. S. Paulson, T.F. Pedersen, H.A. Madsen and F. Rasmussen (2009), *A novel floating offshore wind turbine concept*, Proceedings of the 2009 European Wind Energy Conference, Marseille, France.

/2/ Milestone 11, Work Package 6, DEEPWIND project.

/3/ Hoerner, S- F- and H. V. *Borst, Fluid-Dynamic Lift*. Bricktown, NJ: Hoerner Fluid Dynamics, 1975.

/4/ E. Achenbach and E. *Heinecke (1981). On vortex shedding from smooth and rough cylinders in the range of Reynolds numbers* 6×10^3 *to* 5×10^6. Journal of Fluid Mechanics, 109, pp 239-251 doi:10.1017/S002211208100102X.

/5/ B. M. Sumer and J. Fredsøe (1997), *Hydrodynamics around cylindrical structures*, World Scientific, Advanced Series on Coastal Engineering – Volume 12.

/6/ T. Theodorsen and A. Kegier (1945), *Experiments on drag of revolving disks, cylinders, and streamline rods at high speeds*, National Advisory Committee for Aeronautics, Report no. 793.

/7/ R. I. Basu (1985). *Aerodynamic Forces on Structures of Circular Cross-section. Part 1. Model-scale Data obtained under two-dimensional conditions in low-turbulence streams*. Journal of Wind Engineering and Industrial Aerodynamics, 21, pp 273-294.

/8/ AZoM.com (the A to Z of Materials). *Particle size – US Sieve Series and Tyler Mesh Size equivalents.* http://www.azom.com/article.aspx?ArticleID=1417. May 15, 2002.

/9/ I. G. Currie (1993). *Fundamental Mechanics of Fluids*. 2nd ed., McGraw-Hill Book Co.

/9/ Milne-Thomson, L.M. (1962), Theoretical Hydrodynamics. Macmillan.

D R A W I N G S

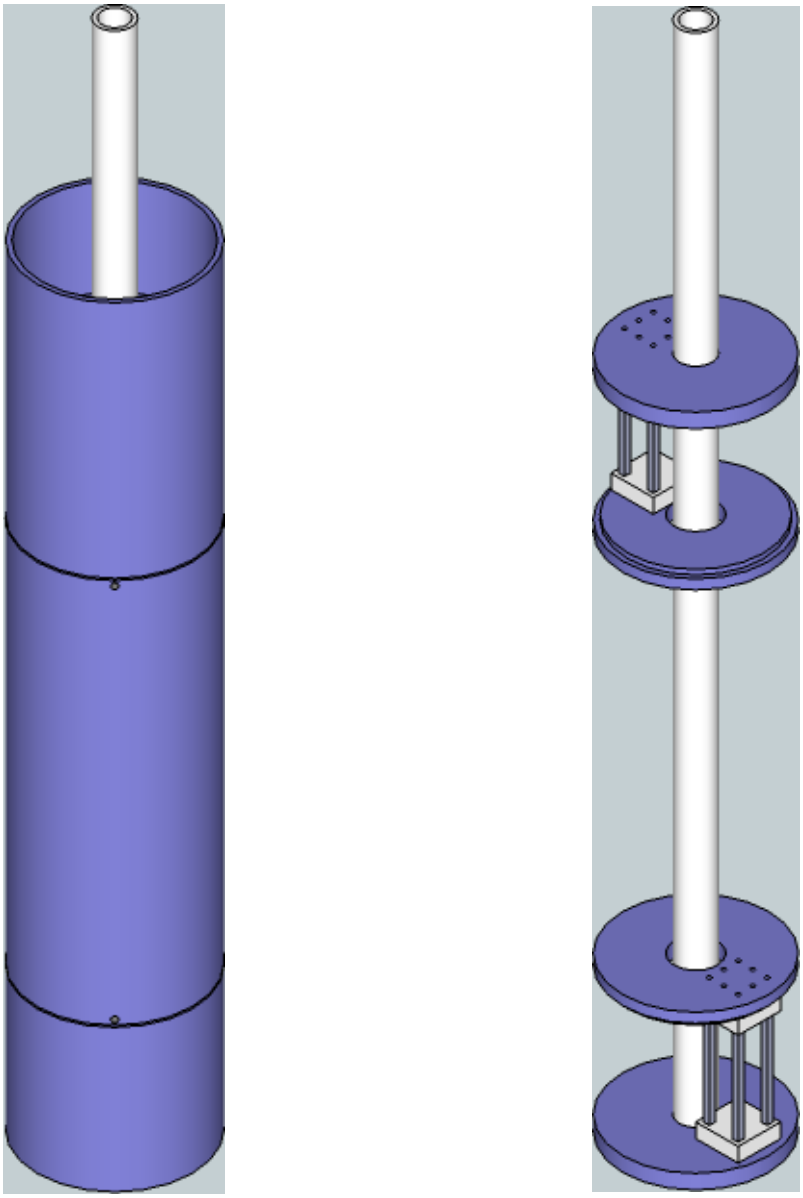

Drawing 1 *(Left) assembled cylinder and (right) shells removed: Top and bottom disks are rigidly fixed to the drive shaft (outer diameter: 33.7 mm, wall thickness: 4.05 mm). Top and bottom cap of measuring section can move relative to the drive shaft.*

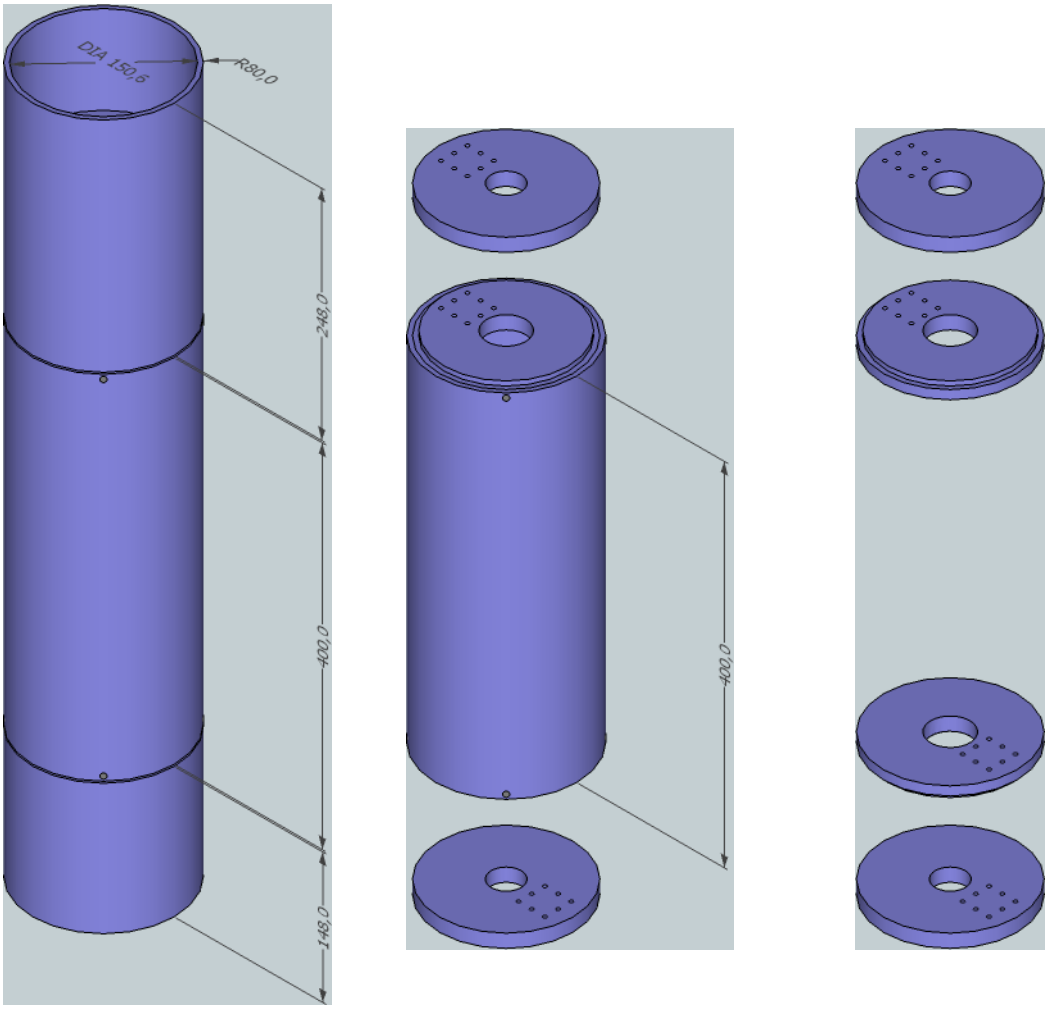

Drawing 2 *(Left) dimensions of the cylinder shells, (middle) position of top cap of measuring section and (right) shells removed.*

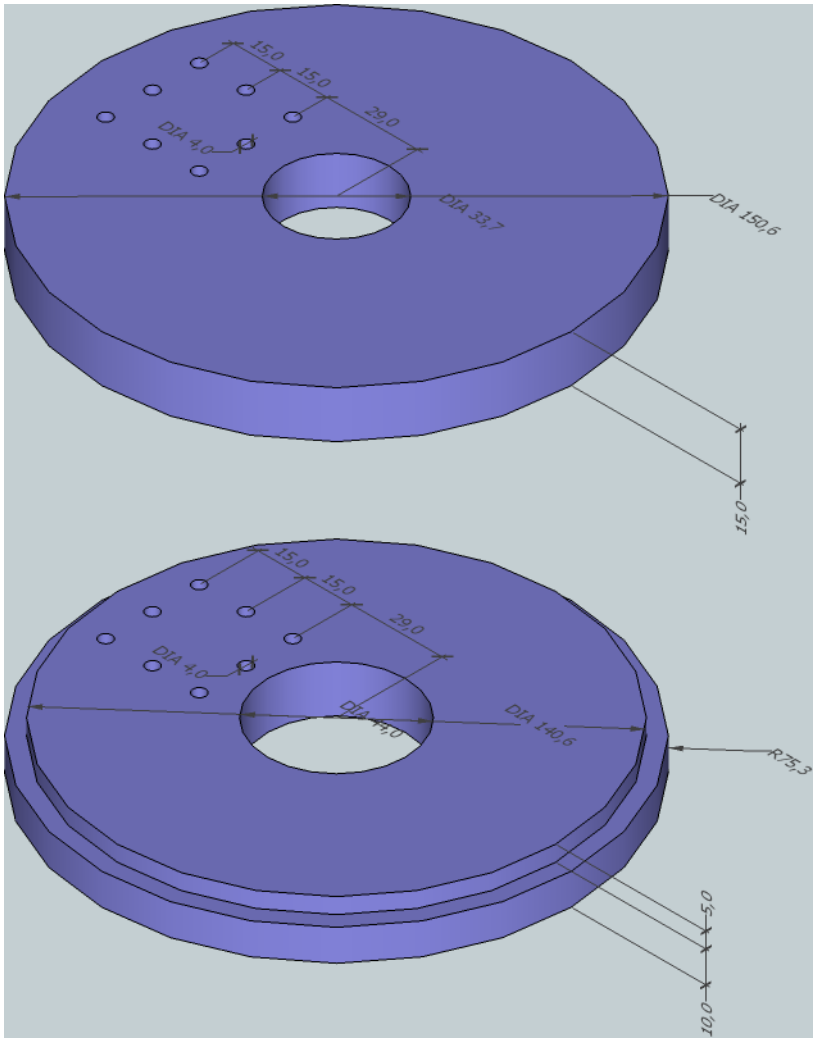

Drawing 3 Dimensions of top and bottom disks/caps

A P P E N D I C E S

A P P E N D I X A

Test Conditions and Force Coefficients

A.1 Current alone

Table A.1 Test conditions and results. Current alone tests.

Test No.	U_c	Re_c	C_D	C_L
		$= D \cdot U_c / v$		
(-)	(m/s)	(-)	(-)	(-)
508	0.064	10204	1.09	-0.05
509	0.099	15804	1.00	0.00
510	0.100	16035	0.97	-0.01
511	0.144	22965	1.05	-0.01
512	0.191	30505	1.05	-0.01
513	0.235	37523	1.08	0.01
514	0.253	40462	1.08	0.01
515	0.314	50212	1.13	0.01
516	0.366	58510	1.15	0.00
517	0.415	66336	1.16	0.04
518	0.458	73219	1.11	0.09
519	0.508	81351	1.00	0.09
520	0.511	81685	1.00	0.08
521	0.573	91666	0.79	0.42
522	0.573	91602	0.79	0.42
523	0.702	112277	0.68	-0.07
524	0.703	112426	0.69	-0.07
525	0.660	105668	0.67	-0.05
526	0.633	101215	0.65	-0.03
527	0.595	95203	0.74	0.30
528	0.595	95241	0.75	0.30
529	0.548	87686	0.85	0.29
530	0.518	82860	0.96	0.12
531	0.435	69636	1.13	0.03

A.2 Wave alone

Table A.2 Test conditions and results. Wave alone tests.

Test	T	U_m	KC	RE	β	C_D	$C_{m,X}$	δ
			$= U_mT/D$	$= D \cdot U_m/v$	= RE/KC			
(-)	(s)	(m/s)	(-)	(-)	(-)	(-)	(-)	(%)
445	1.74	0.14	1.5	21866	14705	0.69	2.02	3.2
446	1.74	0.21	2.3	33482	14711	0.52	2.04	1.4
448	2.14	0.24	3.2	38612	11965	0.49	2.06	1.0
449	2.34	0.26	3.9	42347	10939	0.49	2.07	0.8
450	2.00	0.23	2.9	36736	12800	0.53	2.05	1.5
451	2.47	0.28	4.3	45013	10364	0.55	2.01	0.8
452	2.47	0.28	4.3	44511	10365	0.53	2.02	0.7
453	2.65	0.30	4.9	47283	9662	0.63	2.03	0.7
454	2.76	0.31	5.3	49515	9275	0.56	1.98	0.7
455	2.92	0.33	6.0	52287	8769	0.67	1.97	0.9
456	3.00	0.34	6.4	54276	8533	0.72	1.95	0.9
457	3.27	0.36	7.4	57804	7828	0.79	1.87	0.8
458	3.49	0.39	8.4	61627	7338	0.89	1.81	0.7
459	3.70	0.41	9.4	64972	6919	0.93	1.73	1.1
460	3.90	0.43	10.4	68383	6563	1.00	1.68	1.3
461	4.10	0.45	11.4	71276	6244	1.08	1.61	1.5
462	4.27	0.47	12.4	74589	5996	1.10	1.56	1.5
483	1.74	0.31	3.4	49752	14716	0.55	2.07	0.6
484	2.14	0.32	4.3	50940	11966	0.51	2.02	0.9
485	2.47	0.40	6.3	64798	10366	0.76	1.90	0.6
486	3.00	0.49	9.3	79176	8532	1.10	1.66	0.9
487	3.26	0.53	10.8	84821	7853	1.18	1.63	1.0
488	3.49	0.56	12.3	90264	7336	1.34	1.45	1.6
489	3.70	0.60	13.8	95667	6921	1.26	1.50	1.4
490	2.76	0.45	7.8	72403	9276	0.94	1.76	0.7
493	1.74	0.39	4.2	61826	14713	0.67	2.04	0.8
494	2.14	0.47	6.3	74986	11966	0.86	1.88	0.6
495	2.47	0.54	8.3	85774	10365	1.13	1.71	0.7
497	1.74	0.17	1.8	27186	14714	0.48	2.10	2.1
498	1.74	0.07	0.8	11730	14714	0.46	2.16	6.8
979	4.02	0.44	11.1	70521	6368	1.02	1.62	1.4
981	4.55	0.44	12.5	70421	5626	0.97	1.59	2.3
982	5.15	0.44	14.2	70376	4971	0.94	1.62	1.5
983	6.36	0.44	17.5	70305	4025	0.82	1.74	1.0
984	7.57	0.44	20.8	70468	3383	0.77	1.81	0.9
993	6.36	0.44	17.5	70432	4024	0.80	1.77	0.9
996	5.15	0.44	14.1	70179	4968	0.84	1.73	1.0
1004	5.15	0.44	14.2	70406	4971	0.89	1.67	0.9
1005	4.02	0.44	11.0	70362	6368	1.02	1.63	1.6
1011	2.88	0.44	7.9	70601	8889	0.97	1.73	0.7
1017	3.41	0.44	9.4	70447	7507	0.93	1.64	1.0
1033	8.80	0.44	24.1	69981	2908	0.78	1.76	0.9

A.3 Rotation alone

Table A.3 Test conditions and results. Rotation alone tests

Test No.	ω	Re_ω	$\log_{10}(Re_\omega)$	C_f	$\log_{10}(C_f)$
		$= \omega \cdot R^2/v$			
(-)	(rad/s)	(-)	(-)	(-)	(-)
468	2,09	13364	4,13	0,00603	-2,22
469	2,81	17980	4,25	0,00587	-2,23
470	3,69	23596	4,37	0,00608	-2,22
471	4,57	29254	4,47	0,00589	-2,23
472	5,61	35906	4,56	0,00574	-2,24
473	6,35	40628	4,61	0,00558	-2,25
474	7,16	45803	4,66	0,00533	-2,27
475	8,00	51196	4,71	0,00549	-2,26
476	8,70	55695	4,75	0,00530	-2,28
477	9,39	60123	4,78	0,00537	-2,27

A.4 Current with Rotation

Table A.4 Test conditions and results. Current with rotation tests

Test No.	U_c	Re_c	ω	α	C_D	C_L
		$= D*U_c/v$		$=\omega \cdot R/U_c$		
(-)	(m/s)	(-)	(rad/s)	(-)	(-)	(-)
374	0.350	56050	0.000	0.00	1.16	0.03
375	0.348	55642	2.050	0.47	0.89	-0.09
376	0.348	55638	2.987	0.69	0.84	0.42
377	0.348	55680	3.763	0.87	0.84	0.89
378	0.348	55695	4.572	1.05	0.84	1.32
379	0.346	55298	5.477	1.27	0.87	1.84
380	0.343	54953	6.349	1.48	0.90	2.47
381	0.344	55066	7.068	1.64	0.99	3.01
382	0.341	54638	7.845	1.84	1.16	3.71
383	0.352	56368	0.000	0.00	1.15	0.01
188	0.064	10169	2.499	3.15	2.51	9.42
190	0.063	10011	3.727	4.77	3.83	12.77
191	0.061	9731	4.677	6.15	4.99	15.38
194	0.092	14673	3.138	2.74	1.90	7.65
195	0.090	14324	4.775	4.27	3.42	11.48
197	0.090	14380	6.580	5.86	4.66	14.70
200	0.153	24508	3.148	1.64	0.88	3.07
201	0.152	24321	4.870	2.56	1.82	6.45
272	0.147	23541	3.087	1.68	0.80	3.25
284	0.140	22426	4.803	2.74	1.99	7.32
297	0.148	23697	6.899	3.73	2.99	9.99
318	0.234	37401	4.980	1.70	0.91	3.29
331	0.227	36393	7.071	2.49	2.10	5.89
344	0.225	35933	8.462	3.01	3.01	7.12

A.5 Wave with Rotation

Table A.5 Test conditions and results. Wave with rotation tests

Test	T	U_m	KC =	Re =	ω	α	C_D	$C_{m,X}$	C_L	$C_{m,Y}$
			$U_m \cdot T/D$	$D \cdot U_m/v$		$\omega R/U_m$				
(-)	(s)	(m/s)	(-)	(-)	rad/s	(-)	(-)	(-)	(-)	(-)
121	1.74	0.20	2.2	32323	4.80	1.90	0.44	2.03	3.69	0.16
122	2.14	0.26	3.4	40973	4.71	1.47	0.58	1.97	3.57	0.15
123	2.47	0.27	4.2	43854	4.65	1.36	0.82	2.09	3.62	0.02
124	2.47	0.28	4.2	44014	4.61	1.34	1.07	2.09	3.60	-0.12
125	3.00	0.23	4.3	36920	4.59	1.59	0.57	1.97	4.03	0.23
126	1.74	0.14	1.5	21752	4.55	2.68	0.87	1.95	4.95	0.10
128	1.74	0.39	4.2	61663	4.43	0.92	0.55	2.04	2.86	0.13
129	2.14	0.46	6.2	74185	4.36	0.75	0.72	1.95	2.26	0.20
130	2.47	0.53	8.2	85244	4.25	0.64	1.12	1.87	1.88	0.10
131	2.47	0.53	8.2	84960	5.99	0.90	0.92	2.04	2.73	0.19
150	1.74	0.20	2.2	32241	6.75	2.68	1.11	2.02	4.77	0.23
152	2.14	0.26	3.5	41334	6.67	2.06	0.75	1.96	4.38	0.28
153	2.47	0.28	4.3	44127	6.40	1.86	1.05	2.13	4.55	0.09
156	3.00	0.23	4.3	36856	6.39	2.22	0.72	1.96	4.84	0.35
157	1.74	0.38	4.2	61583	6.19	1.29	0.60	2.06	3.63	0.22
158	2.14	0.46	6.2	74373	6.03	1.04	0.77	1.95	2.89	0.23
159	2.47	0.53	8.2	84950	5.79	0.87	1.22	2.00	2.52	0.02
162	1.74	0.13	1.4	20694	6.93	4.28	1.44	2.04	5.77	0.25
163	1.74	0.13	1.4	20697	8.24	5.10	2.09	2.07	6.91	0.26
164	3.00	0.23	4.3	36450	8.05	2.83	0.77	1.98	5.64	0.41
165	1.74	0.20	2.2	32544	7.86	3.09	0.48	2.05	5.36	0.34
166	2.14	0.26	3.4	41234	7.84	2.43	0.76	2.00	5.21	0.26
167	2.47	0.28	4.3	44126	7.72	2.24	1.26	2.15	5.06	0.03
168	1.74	0.39	4.2	61811	7.43	1.54	0.55	2.07	4.09	0.27
169	2.14	0.46	6.2	74007	7.21	1.25	0.81	1.97	3.25	0.28
170	2.47	0.53	8.2	85127	7.22	1.09	1.07	2.10	3.04	0.10
173	1.74	0.13	1.4	20983	3.19	1.95	0.28	2.06	3.09	0.15
174	3.00	0.23	4.3	37007	3.14	1.09	0.42	1.98	2.94	0.21
175	1.74	0.20	2.2	32345	3.10	1.23	0.31	2.07	2.53	0.16
176	2.14	0.26	3.5	41525	3.08	0.95	0.45	2.00	2.64	0.15
177	2.47	0.28	4.3	44222	3.01	0.87	0.64	2.06	2.73	0.04
178	1.74	0.39	4.2	61929	2.84	0.59	0.63	2.03	2.04	0.13
179	2.14	0.32	4.3	50886	2.91	0.73	0.33	1.98	2.40	0.16
180	2.14	0.46	6.2	74317	2.77	0.48	0.78	1.91	1.52	0.25
181	2.47	0.53	8.2	85056	2.73	0.41	1.10	1.79	1.28	0.19
536	1.74	0.13	1.4	21158	6.04	3.65	N/A	2.03	4.92	0.29
537	1.74	0.13	1.4	20946	7.40	4.52	3.02	2.00	6.23	0.14
538	1.74	0.13	1.4	21266	8.94	5.38	1.27	2.04	6.83	0.29
539	1.74	0.14	1.5	21738	9.71	5.72	2.70	1.96	7.17	0.19
540	1.74	0.39	4.2	61814	1.96	0.41	0.65	2.06	1.49	0.11
541	2.14	0.47	6.3	74809	1.97	0.34	0.82	1.92	1.19	0.19
1097	1.74	0.21	2.2	32996	8.46	3.28	1.89	2.00	5.52	0.16
1114	1.74	0.13	1.4	20701	10.1	6.25	4.16	2.03	7.35	0.24
1115	1.74	0.20	2.2	32548	9.97	3.92	0.41	2.07	5.99	0.45
985	7.57	0.44	20.8	70414	3.16	0.57	0.90	1.80	1.75	0.75
986	7.57	0.44	20.8	70424	4.68	0.85	0.95	1.96	2.38	0.89
987	7.57	0.44	20.8	70512	6.67	1.21	0.94	2.07	3.20	0.29
988	7.57	0.44	20.8	70471	7.96	1.45	1.10	1.50	3.79	-0.40
989	6.36	0.44	17.5	70308	7.91	1.44	1.07	1.44	3.74	-0.16

Test	T	U_m	KC =	Re =	ω	α	C_D	$C_{m,X}$	C_L	$C_{m,Y}$
			$U_m \cdot T/D$	$D \cdot U_m/v$		$\omega R/U_m$				
(-)	(s)	(m/s)	(-)	(-)	rad/s	(-)	(-)	(-)	(-)	(-)
990	6.36	0.44	17.4	69995	4.27	0.78	0.84	1.83	2.49	0.46
991	6.36	0.44	17.4	70216	6.23	1.13	0.91	1.75	3.15	0.02
992	6.36	0.44	17.5	70273	2.26	0.41	0.85	1.72	1.57	0.34
999	5.15	0.44	14.1	70302	6.81	1.24	0.81	1.96	3.49	0.23
1001	5.15	0.44	14.1	70329	8.20	1.49	0.97	1.48	3.90	0.01
1002	5.15	0.44	14.1	70268	4.34	0.79	0.82	1.90	2.52	0.42
1003	5.15	0.44	14.2	70363	2.32	0.42	0.88	1.73	1.52	0.32
1020	4.02	0.50	12.4	79242	6.76	1.09	0.87	1.94	3.27	0.29
1021	4.55	0.44	12.5	70380	6.74	1.23	0.77	1.87	3.43	0.33
1023	4.02	0.56	14.0	89303	6.44	0.92	0.95	1.91	2.86	0.21
1024	4.02	0.62	15.6	99163	6.33	0.82	0.96	1.93	2.60	0.37
1025	5.76	0.44	15.8	70351	6.48	1.18	0.95	1.58	3.27	-0.12
1027	6.97	0.44	19.1	70334	6.45	1.17	1.00	1.63	3.20	-0.14
1028	8.20	0.44	22.4	70049	6.44	1.18	1.01	1.93	3.11	0.51
1029	8.80	0.43	23.9	69589	6.54	1.20	1.02	2.17	3.05	0.79
1030	8.79	0.44	24.1	70184	8.04	1.47	1.05	1.73	3.55	0.02
1031	8.80	0.44	24.1	70250	4.38	0.80	0.92	1.97	2.06	1.01
1032	8.80	0.44	24.1	70161	2.42	0.44	0.87	1.71	1.27	0.65

A.6 Combined Wave and Current with Rotation

Table A.6 Test conditions and results. Combined wave and current with rotation tests

Test	T	U_m	KC = $U_m \cdot T/D$	U_c	ω	α = $\omega R/(U_m+U_c)$	C_D	$C_{m,X}$	C_L	$C_{m,Y}$
(-)	(s)	(m/s)	(-)	(m/s)	rad/s	(-)	(-)	(-)	(-)	(-)
551	1.74	0.13	1.5	0.037	3.09	1.44	0.73	2.04	3.53	0.09
552	1.74	0.20	2.2	0.028	2.92	1.01	0.35	2.09	2.72	0.12
553	2.14	0.26	3.4	0.032	2.84	0.79	0.73	2.02	2.15	0.11
554	3.00	0.23	4.3	0.032	2.81	0.86	0.41	2.02	2.40	0.22
555	2.47	0.28	4.3	0.032	2.75	0.70	0.57	2.04	2.07	0.06
556	2.14	0.32	4.3	0.036	2.74	0.61	0.34	2.00	1.85	0.18
557	1.74	0.32	3.5	0.035	2.78	0.63	0.14	2.05	1.74	0.17
558	2.47	0.41	6.3	0.034	2.68	0.49	0.83	1.98	1.56	0.12
561	1.74	0.13	1.4	0.031	4.91	2.44	0.62	2.06	5.07	0.17
562	1.74	0.21	2.2	0.025	4.78	1.66	0.16	2.05	3.97	0.20
563	2.14	0.26	3.5	0.026	4.70	1.31	0.30	2.00	3.30	0.26
564	3.00	0.23	4.4	0.027	4.67	1.44	0.51	1.99	3.66	0.34
565	2.47	0.28	4.3	0.026	4.65	1.21	0.88	2.05	3.25	0.06
566	2.14	0.32	4.3	0.031	4.62	1.05	0.60	2.00	2.85	0.19
567	1.74	0.32	3.4	0.031	4.50	1.04	0.33	2.06	2.75	0.20
568	2.47	0.41	6.3	0.029	4.43	0.81	0.98	2.08	2.44	0.02
572	1.74	0.13	1.4	0.034	6.72	3.32	1.81	2.07	5.90	0.14
573	1.74	0.21	2.3	0.030	6.62	2.23	0.32	2.01	4.53	0.27
574	2.14	0.26	3.5	0.036	6.54	1.74	0.65	1.93	3.85	0.27
575	3.00	0.23	4.4	0.034	6.54	1.95	0.63	1.95	4.23	0.40
576	2.47	0.28	4.3	0.032	6.44	1.66	1.20	2.14	4.21	0.02
577	2.14	0.32	4.3	0.029	6.19	1.42	0.62	1.97	3.54	0.27
578	1.74	0.31	3.4	0.027	6.23	1.47	0.49	2.07	3.74	0.24
579	2.47	0.41	6.3	0.027	6.08	1.12	1.12	2.13	3.10	0.02
583	1.74	0.13	1.5	0.035	8.41	3.99	2.29	2.01	6.14	0.13
584	1.74	0.20	2.2	0.030	8.25	2.83	0.28	2.06	5.12	0.37
585	2.14	0.26	3.5	0.034	7.85	2.15	0.91	1.98	4.57	0.30
586	3.00	0.23	4.4	0.032	7.44	2.24	0.68	1.97	4.68	0.42
586	3.00	0.23	4.4	0.032	7.44	2.24	0.68	1.97	4.68	0.42
587	2.14	0.32	4.2	0.034	7.29	1.66	0.71	1.99	3.91	0.29
588	1.74	0.32	3.4	0.033	7.16	1.63	0.52	2.02	3.87	0.29
589	2.47	0.28	4.3	0.029	6.96	1.80	0.99	2.15	4.42	0.14
590	2.47	0.41	6.3	0.033	6.90	1.25	0.78	2.21	3.56	0.16
616	1.74	0.14	1.5	0.085	4.66	1.67	0.91	1.91	3.98	0.09
617	1.74	0.20	2.2	0.081	4.61	1.30	0.86	2.03	3.23	0.13
618	2.14	0.26	3.5	0.080	4.56	1.07	0.56	1.92	2.79	0.24
619	3.00	0.23	4.3	0.078	4.55	1.18	0.48	1.89	3.14	0.39
620	2.47	0.28	4.3	0.074	4.54	1.02	0.61	1.96	2.70	0.21
621	1.74	0.32	3.4	0.076	4.40	0.90	0.25	1.98	2.28	0.29
622	2.14	0.32	4.2	0.077	4.37	0.89	0.45	1.93	2.35	0.33
623	2.47	0.41	6.3	0.071	4.35	0.73	0.84	1.94	1.97	0.24
648	1.74	0.13	1.5	0.078	7.14	2.70	1.02	1.99	5.98	0.30
649	1.74	0.20	2.2	0.073	6.89	1.99	1.49	1.99	4.68	0.07
650	2.14	0.26	3.5	0.071	6.75	1.63	0.80	1.94	3.99	0.26
651	3.00	0.24	4.4	0.070	6.74	1.77	0.65	1.92	4.26	0.37
652	2.14	0.32	4.3	0.071	6.54	1.34	0.71	1.91	3.40	0.29
653	1.74	0.31	3.4	0.069	6.51	1.37	0.95	1.99	3.57	0.17
654	2.47	0.28	4.3	0.065	6.51	1.52	1.03	2.08	4.02	0.14
655	2.47	0.41	6.3	0.064	6.18	1.05	1.09	2.09	2.90	0.11

Test	T	U_m	KC = $U_m \cdot T/D$	U_c	ω	α = $\omega R/(U_m+U_c)$	C_D	$C_{m,X}$	C_L	$C_{m,Y}$
(-)	(s)	(m/s)	(-)	(m/s)	rad/s	(-)	(-)	(-)	(-)	(-)
629	1.74	0.13	1.4	0.079	8.11	3.06	0.41	1.97	6.24	0.50
630	1.74	0.21	2.2	0.073	8.02	2.30	0.65	2.01	4.98	0.33
631	2.14	0.26	3.5	0.071	7.98	1.91	0.76	1.91	4.30	0.32
632	3.00	0.23	4.3	0.069	8.04	2.14	0.69	1.96	4.81	0.43
275	2.14	0.26	3.5	0.147	2.62	0.52	0.36	1.81	1.40	0.24
276	2.47	0.28	4.3	0.145	2.51	0.48	0.56	1.78	1.36	0.07
277	3.00	0.23	4.3	0.146	2.55	0.54	0.61	1.66	1.45	0.20
279	2.14	0.32	4.2	0.143	2.50	0.44	0.55	1.80	1.24	0.20
280	2.47	0.40	6.2	0.142	2.49	0.36	0.69	1.76	1.06	0.18
281	1.74	0.32	3.4	0.144	2.53	0.44	0.61	1.87	1.30	0.13
285	1.74	0.13	1.5	0.139	4.72	1.38	1.01	1.87	3.86	0.07
286	1.74	0.20	2.2	0.142	4.59	1.07	0.70	1.95	2.76	0.16
287	2.14	0.26	3.5	0.141	4.50	0.90	0.61	1.78	2.36	0.26
288	2.47	0.28	4.3	0.138	4.42	0.84	0.82	1.80	2.29	0.09
289	3.00	0.23	4.4	0.141	4.54	0.97	0.86	1.68	2.70	0.17
291	2.14	0.32	4.3	0.141	4.51	0.78	0.60	1.75	2.06	0.28
292	2.47	0.41	6.3	0.135	4.43	0.65	0.78	1.81	1.75	0.17
294	1.74	0.32	3.4	0.140	4.50	0.79	0.64	1.87	2.15	0.21
298	1.74	0.13	1.5	0.147	6.53	1.86	1.47	1.88	4.98	0.02
299	1.74	0.20	2.2	0.149	6.43	1.45	1.15	1.89	3.65	0.07
300	2.14	0.26	3.5	0.148	6.31	1.23	0.89	1.76	3.17	0.19
302	3.00	0.23	4.4	0.148	6.29	1.32	1.11	1.73	3.73	0.04
303	2.14	0.32	4.3	0.150	6.17	1.05	0.72	1.77	2.77	0.29
304	1.74	0.32	3.4	0.147	6.18	1.07	0.75	1.86	2.89	0.22
305	2.47	0.41	6.3	0.144	6.07	0.88	0.99	1.78	2.44	0.15
319	1.75	0.13	1.4	0.231	4.49	1.00	1.47	1.25	2.65	-0.87
320	1.74	0.20	2.2	0.230	4.44	0.82	0.93	1.74	2.34	-0.07
321	2.14	0.26	3.4	0.232	4.48	0.73	0.88	1.62	2.07	0.07
322	2.47	0.28	4.3	0.231	4.43	0.70	1.04	1.52	2.09	-0.13
323	3.00	0.23	4.4	0.229	4.44	0.77	1.13	1.52	2.42	-0.10
324	2.14	0.32	4.3	0.233	4.33	0.63	0.73	1.59	1.71	0.26
325	1.74	0.32	3.4	0.231	4.32	0.63	0.71	1.71	1.70	0.18
326	2.47	0.41	6.3	0.229	4.33	0.54	0.96	1.58	1.55	0.08
332	1.74	0.13	1.4	0.228	6.83	1.52	1.44	1.75	4.16	-0.18
333	1.74	0.20	2.2	0.226	6.49	1.21	1.22	1.74	3.35	-0.13
334	2.14	0.26	3.5	0.226	6.54	1.07	1.07	1.58	2.97	-0.07
335	3.00	0.23	4.4	0.225	6.49	1.13	1.29	1.70	3.32	-0.24
336	2.47	0.28	4.3	0.228	6.31	0.99	1.37	1.57	2.95	-0.29
338	2.14	0.32	4.3	0.229	6.13	0.89	0.90	1.61	2.52	0.13
339	1.74	0.32	3.4	0.227	5.97	0.88	1.00	1.66	2.39	-0.02
340	2.47	0.41	6.3	0.224	6.12	0.78	1.23	1.67	2.31	0.07
345	1.74	0.13	1.4	0.226	7.74	1.74	1.58	1.84	4.60	-0.12
346	1.74	0.21	2.2	0.224	7.93	1.47	1.31	1.74	3.68	-0.13
347	2.14	0.26	3.5	0.229	7.77	1.27	1.17	1.55	3.37	-0.13
348	3.00	0.23	4.4	0.228	7.25	1.26	1.27	1.72	3.55	-0.24
349	2.47	0.28	4.3	0.229	7.72	1.22	1.54	1.57	3.35	-0.41
350	2.14	0.32	4.3	0.230	7.67	1.11	1.15	1.55	3.02	-0.11
351	1.74	0.32	3.5	0.230	7.63	1.11	0.99	1.72	2.82	0.07
352	2.47	0.41	6.3	0.227	7.56	0.95	1.39	1.67	2.76	0.06
386	1.74	0.13	1.4	0.344	4.62	0.77	1.35	1.32	1.77	-0.06
387	1.74	0.21	2.3	0.348	4.58	0.66	1.31	1.38	1.75	-0.08
388	2.14	0.26	3.4	0.351	4.52	0.59	1.15	1.50	1.87	-0.01

Test	T	U_m	KC = $U_m \cdot T/D$	U_c	ω	α = $\omega R/(U_m+U_c)$	C_D	$C_{m,X}$	C_L	$C_{m,Y}$
(-)	(s)	(m/s)	(-)	(m/s)	rad/s	(-)	(-)	(-)	(-)	(-)
389	3.00	0.23	4.4	0.352	4.52	0.62	1.27	1.60	1.80	0.76
390	2.47	0.28	4.3	0.352	4.52	0.57	1.30	1.57	2.01	-0.18
392	2.14	0.32	4.2	0.354	4.26	0.51	1.10	1.52	1.64	0.07
393	1.74	0.31	3.4	0.355	4.49	0.54	1.28	1.47	1.62	0.01
394	3.00	0.34	6.4	0.356	4.48	0.52	1.25	1.55	1.58	0.68
398	1.74	0.13	1.4	0.345	6.45	1.08	1.41	1.37	2.63	-0.43
399	1.74	0.21	2.3	0.350	6.37	0.91	1.31	1.43	2.52	-0.22
400	2.14	0.26	3.5	0.349	6.35	0.83	1.33	1.59	2.66	-0.37
401	3.00	0.23	4.4	0.350	6.19	0.85	1.32	1.72	2.23	0.77
402	2.47	0.28	4.3	0.350	6.31	0.80	1.37	1.69	2.47	-0.02
403	2.14	0.32	4.3	0.351	6.27	0.75	1.24	1.65	2.46	-0.10
405	1.74	0.32	3.4	0.352	6.27	0.75	1.30	1.47	2.34	-0.19
406	3.60	0.29	6.4	0.350	6.28	0.79	1.26	1.52	1.87	1.27
410	1.74	0.14	1.5	0.336	7.92	1.34	1.49	1.51	3.57	-0.22
411	2.14	0.11	1.5	0.337	8.16	1.45	1.60	1.62	3.72	-0.69
412	2.47	0.10	1.5	0.335	8.05	1.48	1.59	1.86	3.69	-0.33
413	1.74	0.11	1.1	0.337	7.70	1.39	1.46	1.31	3.26	-0.38
414	3.00	0.08	1.5	0.338	7.59	1.45	1.37	2.33	3.26	2.22
415	1.74	0.21	2.2	0.339	7.88	1.16	1.53	1.48	3.29	-0.36
416	2.14	0.26	3.4	0.341	7.88	1.05	1.48	1.62	3.17	-0.39
417	3.00	0.23	4.4	0.341	7.87	1.10	1.44	1.88	2.77	0.79
418	2.47	0.28	4.3	0.344	7.86	1.01	1.48	1.69	2.89	-0.01
422	1.74	0.13	1.5	0.343	2.84	0.48	1.25	1.33	0.88	-0.01
423	1.74	0.21	2.3	0.348	2.79	0.40	1.32	1.33	0.91	-0.11
424	2.14	0.26	3.5	0.348	2.77	0.36	1.18	1.41	1.02	-0.09
425	3.00	0.23	4.3	0.348	2.80	0.39	1.09	1.50	1.19	0.31
426	2.47	0.28	4.3	0.349	2.80	0.36	1.07	1.50	1.28	-0.14
427	2.14	0.32	4.2	0.351	2.77	0.33	1.17	1.48	1.08	-0.02
428	1.74	0.31	3.4	0.351	2.75	0.33	1.26	1.46	1.00	0.01
429	2.47	0.41	6.3	0.357	2.72	0.28	1.07	1.45	0.91	0.11

A P P E N D I X B

US Sieve Series and Tyler Mesh Size Equivalents

Table B.1 US Sieve Series and Tyler Mesh Size Equivalents. Reproduced from AZom.com /8/.

US Sieve Series	Tyler Equivalent	Opening (mm)
-	2½ Mesh	8.00
-	3 Mesh	6.73
No. 3½	3½ Mesh	5.66
No. 4	4 Mesh	4.76
No. 5	5 Mesh	4.00
No. 6	6 Mesh	3.36
No. 7	7 Mesh	2.83
No. 8	8 Mesh	2.38
No.10	9 Mesh	2.00
No. 12	10 Mesh	1.68
No. 14	12 Mesh	1.41
No. 16	14 Mesh	1.19
No. 18	16 Mesh	1.00
No. 20	20 Mesh	0.841
No. 25	24 Mesh	0.707
No. 30	28 Mesh	0.595
No. 35	32 Mesh	0.500
No. 40	**35 Mesh**	**0.420**
No. 45	42 Mesh	0.354
No. 50	48 Mesh	0.297
No. 60	60 Mesh	0.250
No. 70	65 Mesh	0.210
No. 80	80 Mesh	0.177
No.100	**100 Mesh**	**0.149**
No. 120	115 Mesh	0.125
No. 140	150 Mesh	0.105
No. 170	170 Mesh	0.088
No. 200	200 Mesh	0.074
No. 230	250 Mesh	0.063
No. 270	270 Mesh	0.053
No. 325	325 Mesh	0.044
No. 400	400 Mesh	0.037

A P P E N D I X C

Potential Flow Solution

C.1 Definitions

The *complex potential* is defined:

$$W(z) = \varphi(x,y) + i\psi(x,y)$$

where $z = x + iy$, φ is the velocity potential and ψ is the stream function. The derivative of W with respect to z is the complex (conjugate) velocity:

$$\frac{dW}{dz} = u_x - iu_y = (u_r - iu_\theta)e^{-i\theta}$$

where u_x is the velocity in the *x*-direction and u_y is the *y*-direction. In terms of the two cylindrical terms the Cartesian velocity components may be expressed as:

$$u_x = u_r cos\theta - u_\theta sin\theta$$

$$u_y = u_r sin\theta + u_\theta cos\theta$$

Substituting these expressions into the complex velocity gives d*W*/dz in terms of u_r and u_θ.

C.2 Accelerated Circular Cylinder with Circulation

Suppose a cylinder of radius R placed at position z_0 is moving through a 2D ideal fluid along the x-axis at instantaneous velocity, $dz_0/dt = dx_0/dt = U$. In a (primed, $z' = z - z_0$) coordinate system moving with the cylinder and with zero at z_0 it appears to be the fluid that passes by the fixed cylinder at velocity –U. In the absence of the cylinder the complex potential in the primed coordinated would be given by $dW'/dz' = u_x' - iu_y' = -U$, so that $W' = -Uz'$. Applying the *Milne-Thomson circle theorem* the complex potential in the presence of the cylinder is then:

$$W' = -Uz' + \overline{\left(-U\frac{R^2}{\overline{z'}}\right)} = -Uz' - U\frac{R^2}{z'}$$

The instantaneous flow expressed in the primed and fixed (non-primed) coordinates is related by:

$$\frac{dW'}{dz'} = \frac{dW}{dz} - U$$

and thus (apart from a constant):

$$W = W' + Uz' = -U\frac{R^2}{z - z_0}$$

Now add a point vortex of strength Γ at position z_0. It contributes to the complex potential by the second term on the right-hand side in the equation below to give the complex potential for a rotating cylinder moving with velocity, *U*, in an otherwise still fluid,

$$W = -U\frac{R^2}{z - z_0} - i\frac{\Gamma}{2\pi}\log(z - z_0)$$

The corresponding complex velocity becomes:

$$\frac{dW}{dz} = U\frac{R^2}{(z - z_0)^2} - i\frac{\Gamma}{2\pi}\frac{1}{(z - z_0)}$$

Setting $z - z_0 = r(cos\theta + isin\theta) = re^{i\theta}$ the complex velocity becomes:

$$\frac{dW}{dz} = \left(U\frac{R^2}{r^2}e^{-i\theta} - i\frac{\Gamma}{2\pi r}\right)e^{-i\theta}$$

$$= \left(U\frac{R^2}{r^2}(cos\theta - isin\theta) - i\frac{\Gamma}{2\pi r}\right)e^{-i\theta}$$

$$= (U\frac{R^2}{r^2}cos\theta - i(U\frac{R^2}{r^2}sin\theta + \frac{\Gamma}{2\pi r}))e^{-i\theta}$$

Hence, by comparison with the complex velocity expressed in terms of u_r and u_θ the velocity components are:

$$u_r = U\frac{R^2}{r^2}cos\theta$$

$$u_\theta = U\frac{R^2}{r^2}sin\theta + \frac{\Gamma}{2\pi r}$$

C.2.1 Pressures around the Cylinder and Resultant Force

The pressure around the cylinder can be calculated, employing the general Bernoulli equation (/9/):

$$\frac{p}{\rho} + \frac{1}{2}u^2 - \frac{\partial\varphi}{\partial t} = \text{constant}$$

in which u is the speed

$$u^2 = u_r^2 + u_\theta^2 = (U\frac{R^2}{r^2}cos\theta)^2 + (U\frac{R^2}{r^2}sin\theta + \frac{\Gamma}{2\pi r})^2$$

on the cylinder surface where $r = R$ the speed will be:

$$u^2|_{r=R} = (Ucos\theta)^2 + (Usin\theta + \frac{\Gamma}{2\pi R})^2$$

$$= U^2(cos^2\theta + sin^2\theta)^2 + (\frac{\Gamma}{2\pi R})^2 + \frac{\Gamma U}{\pi R}sin\theta$$

$$= U^2 + (\frac{\Gamma}{2\pi R})^2 + \frac{\Gamma U}{\pi R} sin\theta$$

The velocity potential is the real part of the complex potential and thus:

$$\frac{\partial \varphi}{\partial t} = \Re\left\{\frac{\partial W}{\partial t}\right\}$$

where the time derivative of the complex potential is:

$$\frac{\partial W}{\partial t} = -\frac{dU}{dt}\frac{R^2}{z-z_0} + U\frac{R^2}{(z-z_0)^2}\frac{dz_0}{dt} - i\frac{\Gamma}{2\pi}\frac{1}{(z-z_0)}\frac{dz_0}{dt}$$

$$= -\frac{dU}{dt}\frac{R^2}{z-z_0} + U^2\frac{R^2}{(z-z_0)^2} - i\frac{\Gamma U}{2\pi}\frac{1}{(z-z_0)}$$

Setting $z - z_0 = re^{i\theta}$ and the time derivative of the velocity potential becomes:

$$\frac{\partial \varphi}{\partial t} = \Re\left\{\frac{\partial W}{\partial t}\right\}$$

$$= \Re\left\{-\frac{dU}{dt}\frac{R^2}{r}e^{-i\theta} + U^2\frac{R^2}{r^2}e^{-2i\theta} - i\frac{\Gamma U}{2\pi r}e^{-i\theta}\right\}$$

$$= -\frac{dU}{dt}\frac{R^2}{r}cos\theta + U^2\frac{R^2}{r^2}\cos(2\theta) + i^2\frac{\Gamma U}{2\pi r}sin\theta$$

which on the cylinder surface where $r = R$ becomes:

$$\left.\frac{\partial \varphi}{\partial t}\right|_{r=R} = -R\frac{dU}{dt}cos\theta + U^2\cos(2\theta) - \frac{\Gamma U}{2\pi R}sin\theta$$

Therefore, the pressure on the surface of the cylinder may be written as:

$$p|_{r=R} = -\frac{1}{2}\rho u^2|_{r=R} + \rho\left.\frac{\partial \varphi}{\partial t}\right|_{r=R} + \text{constant}$$

$$= -\frac{1}{2}\rho(\frac{\Gamma U}{\pi R}sin\theta) + \rho(-R\frac{dU}{dt}cos\theta + U^2\cos(2\theta) - \frac{\Gamma U}{2\pi R}sin\theta) + \text{constant}$$

$$= -\rho\frac{\Gamma U}{\pi R}sin\theta - \rho R\frac{dU}{dt}cos\theta + \rho U^2\cos(2\theta) + \text{constant}$$

where the constant term in the second and third lines includes also $\frac{1}{2}\rho U^2$ and $\rho(\Gamma/(2\pi R))^2$.

The resultant force can then be calculated by integrating the pressure around the cylinder:

$$F_x = -\int_0^{2\pi} p\cos\theta(Rd\theta) = \rho\pi R^2 \frac{dU}{dt}$$

$$F_y = -\int_0^{2\pi} p\sin\theta(Rd\theta) = \rho\Gamma U$$

C.2.2 Useful Integrals

In the integration of pressure the following relationships have been utilized:

$$\int_0^{2\pi} \cos^2\theta d\theta = \int_0^{2\pi} \sin^2\theta d\theta = \pi$$

$$\int_0^{2\pi} \cos(m\theta)\cos(n\theta)d\theta = 0 \qquad m, n \text{ integers and } m \neq n$$

$$\int_0^{2\pi} \sin(m\theta)\cos(n\theta)d\theta = 0 \qquad m, n \text{ integers}$$